those in V54KO+GPR108 were 1.23 ± 0.14 and 1.15 ± 0.027 times, respectively, those in V54KO+Vec [$n = 2$]). These results suggested the specific function of TMEM87A and TMEM87B. Because these two proteins have not been characterized, we first investigated their localization in mammalian cells. Because endogenous TMEM87A protein could not be detected by immunoblotting and immunofluorescence analysis in HEK293 cells, expression plasmids of N-terminally hemagglutinin (HA)-tagged or C-terminally 3×HA-tagged TMEM87A and TMEM87B were constructed and their functions confirmed based on their ability to restore the V54KO phenotype. Overexpression of N- or C-terminally tagged TMEM87A restored the impairment of anterograde transport of VFG-GPI to an extent similar to that of the nontagged version (Supplemental Figure S3A), indicating that both HA-tagged TMEM87As were functional; by contrast, neither of the tagged TMEM87Bs was functional. Nontagged or N- or C-terminally HA-tagged TMEM87A was transiently expressed in wild-type cells, and the localization of the proteins was analyzed by confocal microscopy. As shown in Figure 6C, nontagged or N- or C-terminally HA-tagged TMEM87A predominantly colocalized with GPP130, indicating its Golgi localization.

To investigate the mechanism by which TMEM87A overexpression restored anterograde transport in V54KO cells, retrograde transport of CTxB was examined in TMEM87A-overexpressing cells. Thus N-terminally HA-tagged TMEM87A was stably expressed in V54KO cells (V54KO+TM87A), and cells in which anterograde transport of VFG-GPI was partially restored were collected (Supplemental Figure S3B). At 60 min, TGN-localized CTxB levels were significantly higher in V54KO+TM87A cells than in V54KO+Vec cells (Figure 6, D and E), which indicated that the V54KO phenotype could be restored by the restoration of retrograde transport in V54KO cells. Finally, we investigated whether a loss of TMEM87A and B affects retrograde transport of CTxB. For this, we generated TMEM87A and TMEM87B double-KO (TM87A, B-DKO) cell lines using HEK293 cells. HEK293 cells expressed both genes at levels comparable to VPS51 and VPS54 as assessed by quantitative reverse-transcription PCR (qRT-PCR; Supplemental Figure S4A), although TMEM87A protein was not detected by monoclonal anti-TMEM87A antibody and TMEM87B protein could not be tested due to a lack of anti-TMEM87B antibody. Retrograde transport of CTxB was not affected in TM87A, B-DKO cell lines (data with clone #2 shown in Supplemental Figure S4B). It seemed that TMEM87A and B were not directly involved in retrograde transport of CTxB or that yet another protein was redundantly involved. It is therefore likely that overexpression of TMEM87A or B in V54KO cells enhanced retrograde transport efficiency in general. Taken together, our data provide strong evidence that TMEM87A and TMEM87B are Golgi-localized proteins involved in endosome-to-TGN retrograde transport.

DISCUSSION

The aim of this study was to identify genes necessary for the efficient anterograde transport of GPI-APs. Haploid-genetic screening identified genes encoding subunits of the GARP complex. Depletion of each component of this complex revealed its requirement in the anterograde transport of both GPI-anchored and transmembrane proteins. In V54KO cells, post-Golgi anterograde transport was severely delayed, consistent with localization of the GARP complex within the TGN (Perez-Victoria *et al.*, 2008). The delay in anterograde transport in V54KO cells was partially restored by the overexpression of VAMP4 but not VAMP3, which also functions in endosome-to-TGN retrograde transport (Mallard *et al.*, 2002). VAMP4 overexpression also repaired the endosome-to-TGN retrograde transport defect. According to these results, the defective anterograde transport in GARP-KO cells was caused by impaired endosome-to-TGN retrograde transport. In addition, knockdown of VAMP4 or STX6 resulted in the defective anterograde transport of both GPI-anchored and transmembrane proteins. These results support a model in which endosome-to-TGN retrograde transport mediated by VAMP4 and GARP is required for recycling of molecular elements involved in post-Golgi anterograde transport (Supplemental Figure S5). Because anterograde transport of GPI-AP was more efficiently restored than retrograde transport of CTxB in V54KO+VAMP4 cells (Supplemental Figure S2B and Figure 5C), VAMP4 might be one of the factors that are GARP-dependently recycled and essential for the post-Golgi anterograde transport. Indeed, it was reported that the localization of VAMP4 was impaired in GARP-depleted cells (Perez-Victoria and Bonifacino, 2009). Although the possibility that the GARP complex is directly involved in anterograde transport cannot be ruled out, this is unlikely because the overexpression of VAMP2, which forms a complex with plasma membrane–localized t-SNAREs and is required for the post-Golgi anterograde transport of proteins (Calakos *et al.*, 1994; Olson *et al.*, 1997; Chen and Scheller, 2001), could not restore delayed anterograde transport in V54KO cells (Supplemental Figure S2A).

Recently it was reported that members of GARP complex form another protein complex, termed endosome-associated recycling protein (EARP), which is the multisubunit tethering factor required for endocytic recycling (Schindler *et al.*, 2015). In addition to VPS51, VPS52, and VPS53, EARP complex contains syndetin instead of VPS54. We produced VPS51, 52, 53, and 54 KO cells. In the VPS51, 52, or 53 KO cells, both GARP and EARP functions would be impaired. In this study, however, VPS54 KO cells showed defects in anterograde protein transport from the Golgi, suggesting that GARP function itself for tethering of endosome-derived vesicles to the Golgi is important for the transport.

The *COG8* gene, encoding a subunit of the COG complex, was identified in this screening (Figure 1B). Similar to GARP complex, COG complex is a multisubunit tethering factor composed of eight subunits (Ungar *et al.*, 2006). COG complex acts as a tethering complex required for intra-Golgi or endosome-to-TGN retrograde transport (Oka *et al.*, 2004; Laufman *et al.*, 2011). Either or both of these functions of COG might contribute to post-Golgi anterograde transport of integral membrane proteins.

Our results (Figure 5, A–C) are consistent with previous reports showing that both tethering factors and SNAREs, especially v-SNAREs, contribute to vesicle docking and that overexpression of v-SNAREs compensates for tethering defects (VanRheenen *et al.*, 1998; Wiederkehr *et al.*, 2004; Laufman *et al.*, 2011). As discussed by Laufman *et al.* (2011), overexpression of VAMP4 could bypass the requirement for tethering complexes (GARP in our case) because endosome-derived transport vesicles bearing highly concentrated v-SNARE proteins may directly interact with the t-SNARE complex, leading to their fusion (Laufman *et al.*, 2011). Unlike v-SNAREs, however, t-SNAREs have no such activity (Supplemental Figure S2A; Laufman *et al.*, 2011). There are at least three different t-SNARE complexes in the TGN or the Golgi: STX6-STX16-Vti1, STX10-STX16-Vti1, and STX5-Ykt6-GS28. Although distinct functions for these complexes have been proposed (Mallard *et al.*, 2002; Tai *et al.*, 2004; Ganley *et al.*, 2008), there may be partial overlap such that the total amount of t-SNAREs is what allows vesicle tethering and fusion. Consistent with this speculation, the transport delay in cells with a knocked down STX6 was milder than in cells with a knocked down VAMP4 (Figure 5E).

In previous studies, knockdown of VAMP4 or STX6 did not cause delayed anterograde transport of VSVG^{ts} (Choudhury *et al.*, 2006; Shitara *et al.*, 2013). However, we found that the anterograde transport of GPI-anchored and transmembrane reporter proteins was clearly affected by the knockdown of VAMP4 or STX6 (Figure 5E). The discrepancy might be because of the different analytical methods; in the cited work, microscopy-based analyses were used to quantify transport efficiency, whereas we used a flow cytometry–based transport assay. This allowed the simultaneous analysis of >10,000 cells, in addition to being a more sensitive and quantitative method than microscopy. Therefore flow cytometric analysis might be advantageous in the detection of small changes in transport efficiency, such as those seen with STX6 knockdown.

Mutations in the GARP complex have been described in the literature. For example, the *wobbler* mouse, used as a model for amyotrophic lateral sclerosis, has a point mutation in VPS54, leading to neurodegeneration (Schmitt-John *et al.*, 2005; Moser *et al.*, 2013). The *wobbler* mutation causes VPS54 destabilization and leads to impaired endosome-to-TGN retrograde transport (Perez-Victoria *et al.*, 2010a; Karlsson *et al.*, 2013). However, the pathogenic mechanism has yet to be elucidated. More recently, mutations in VPS53 were identified in patients with progressive cerebello-cerebral atrophy type 2 (Feinstein *et al.*, 2014). These patients display cerebellar and cerebral neuronal atrophy before the age of 1 yr. The molecular mechanism leading to progressive cerebello-cerebral atrophy type 2 in patients carrying a mutation in VPS53 is also not understood. Of interest, despite the different phenotypes of VPS53 and VPS54 mutations, motor neurons are affected in both cases (Brunet and Sacher, 2014). In humans, it was reported that mutations in genes involved in anterograde transport of proteins cause motor neuronal diseases (Maruyama *et al.*, 2010; Novarino *et al.*, 2014). Our study revealed the importance of the GARP complex in the post-Golgi anterograde transport of GPI-anchored and transmembrane proteins. In addition to the retrograde transport defect itself, defective anterograde transport resulting from inefficient protein recycling from the endosome to the TGN might contribute to the pathogenic mechanism of disorders caused by VPS53 and VPS54 mutations.

We further screened genes whose overexpression restored delayed anterograde transport in V54KO cells and identified an as-yet-uncharacterized gene, *TMEM87A*, a member of the LU7TM family. Both TMEM87A and its close homologue TMEM87B restored delayed anterograde transport in V54KO cells, suggesting their functional redundancy. Microscopy analysis demonstrated the Golgi localization of TMEM87A, indicating its function at this site. This result is consistent with a previous report in which Ptm1p, the yeast homologue of TMEM87A, was identified in Tlg2p (yeast homologue of STX16)-containing compartments (Inadome *et al.*, 2005). The retrograde transport of CTxB provided proof that transport was partially restored in V54KO+TM87A cells. Thus restoration of the V54KO phenotype by the overexpression of TMEM87A resulted from the restoration of retrograde transport in V54KO cells and suggested the involvement of TMEM87A in endosome-to-TGN retrograde transport (Supplemental Figure S5). Retrograde transport might be a common function of LU7TM family proteins, since it is shared by GPR107, another member of this family. However, our overexpression experiments (Figure 6, A and B) evidenced two functional subfamilies, such that TMEM87A/B and GPR107/108 might be involved in different retrograde transport pathways.

Several questions regarding the precise functions of these LU7TM family proteins and how these proteins are involved in retrograde transport remain unresolved. One possibility is that G protein–coupled receptors (GPCRs) are needed to maintain Golgi homeostasis. In pharmacological studies, Golgi-localized Gβγ was shown to be required for post-Golgi anterograde transport (Stow *et al.*, 1991; Irannejad and Wedegaertner, 2010). However, the GPCRs associated with Golgi-localized Gβγ are not known. Tafesse *et al.* (2014) proposed GPR107 as one such GPCR. In our study, TMEM87A/B modulated both endosome-to-TGN retrograde transport and post-Golgi anterograde transport. Thus TMEM87A and TMEM87B are also good candidate GPCRs. Further studies are needed to elucidate the molecular function of these proteins.

In conclusion, this study showed that GARP- and VAMP4-dependent endosome-to-TGN retrograde transport is required for recycling of molecules critical for the efficient post-Golgi anterograde transport of GPI-anchored and transmembrane proteins. GPI-APs lack a cytoplasmic domain, so their efficient transport probably relies on putative transmembrane cargo receptors. Identification of cargo receptors that recognize GPI-APs would confirm this molecular mechanism.

MATERIALS AND METHODS

Reagents and antibodies

Lipofectamine 2000 and Lipofectamine RNAi MAX were purchased from Life Technologies (Carlsbad, CA). As primary antibodies, we used mouse monoclonal anti-CD59 (clone 5H8; Hirata *et al.*, 2013), anti-FLAG (clone M2), anti-HA (clone HA7; Sigma-Aldrich, St. Louis, MO), anti-STX6 (Stressgen, San Diego, CA), anti–α-tubulin, anti-Golgin97 (clone CDF4; Life Technologies), anti-TMEM87A (clone #772807; R&D Systems, Minneapolis, MN), rabbit monoclonal anti-LAMP1 (clone D2D11; Cell Signaling Technology, Danvers, MA), rabbit polyclonal anti-VPS53, VPS52 (a kind gift from Chris Schindler and Juan Bonifacino, National Institutes of Health, Bethesda, MD; Perez-Victoria *et al.*, 2008), anti-GPP130 (Covance, Princeton, NJ), and anti-EEA1. The secondary antibodies were phycoerythrin (PE)-conjugated goat anti-mouse immunoglobulin G (IgG; BioLegend, San Diego, CA), Alexa Fluor 594–conjugated goat anti-mouse IgG, and Alexa Fluor 647–conjugated goat anti-mouse IgG (Life Technologies). Alexa Fluor 488–conjugated CTxB was purchased from Life Technologies.

Plasmid construction

A DNA fragment of VSVGex-FF-mEGFP-GPI (VFG-GPI), which encodes a GPI reporter protein, was amplified from pME-Neo2dH-VSVGex-FF-mEGFP-GPI (Maeda *et al.*, 2008). The amplified fragment was cloned into the *Not*I and *Mlu*I sites of pRetroX-Tight–puromycin *N*-acetyl-transferase (Pur; Clontech, Palo Alto, CA) using the In-fusion cloning reagents (Takara, Shiga, Japan) to generate pRetroX-VFG-GPI-Pur. A DNA fragment of Flag-VSVG^{full}-EGFP (FVG-TM), encoding a transmembrane reporter protein, was amplified from pME-FLAG-VSVG^{full}-EGFP (Maeda *et al.*, 2008). The amplified fragment was cloned into pRetroX-Tight-Pur using the same method as used to generate pRetroX-FVG-TM-Pur. A retroviral gene-trap vector containing an adenoviral splice acceptor (SA) site, a PGK polyA signal, a PGK promoter (PGKpro), the blasticidin-S deaminase (BSD) gene, and human growth hormone (hGH) polyA was constructed as follows. The adenoviral SA site and hGH polyA sequence were amplified from pCMT-SAhygpA-NP21 (GenBank AB609713; Horie *et al.*, 2011), which was kindly provided by Kyoji Horie (Nara Medical University, Nara, Japan). The primers (SA site) GTTCCTATTCTCTAGAAAGTATAGGAACTTCAGTG and ttGCGGCCGCTCAggTCAgTCAGAATTCCGGCGGCTAGCGATACCGTC, and (hGH polyA) ccTGAGCGGCCGCaaaaATCGATtCTGTGCCTTCTAGTTGCCAGC and TGGACCATCCTCTAGACTGCC, were used in the amplification. The amplified fragments were

cloned into pCMT-SAhygpA-NP21 at the two *Xba*I sites using the In-fusion cloning reagents, generating pCMT-SA. The PGK polyA and PGKpro sequences were amplified from pCMT-SAhygpA-NP21 using primers CTGACCTGAGCGGCCGCAGAAATTGATGATCTATTAAACAATAAAGA and ggtggACGCGTAGGTCGAAAGGCCCGGAGAT. The BSD gene was amplified from pLIB2-pgk-BSD (Maeda *et al.*, 2008) using primers acctACGCGTccaccATGCCTTTGTCTCAAGAAGAATC and GAAGGCACAGAATCGATTTAGCCCTCCCACACATAACC. The resulting PGK polyA-PGKpro and BSD fragments were cloned into the *Not*I and *Cla*I sites of pCMT-SA using In-fusion cloning reagents to generate pCMT-SApA-pgkBSD. The CRISPR/Cas9 expression plasmid, pX330 (Cong *et al.*, 2013), was obtained from Addgene and used to generate pX330-hVPS51, -hVPS52, -hVPS53, -hVPS54#1, and -hVPS54#2; targeting sequences (described later) were cloned into pX330 plasmids digested with *Bbs*I. To construct pX330-mEGFP plasmid, a PCR fragment amplified from a template plasmid, pME-$(G4S)_2$-mEGFP, using primers (gagaGGCCGGCCAaGCtAAgAAaAAgAAaATGACGCGTGGCGGAG and gagaGGCCGGCCTTcTTgGTtGCgGCaGGtCTcTTtccCTTGTACAGCTCGTCCA) was digested with *Fse*I and cloned into the same site of pX330 vector. To generate pX330-mEGFP-hTMEM87A, -hTMEM87B#1, and -hTMEM87B#2, targeting sequences (described later) were cloned into pX330-mEGFP digested with *Bbs*I. To express the GARP complex subunits, pEF6-BSD-VPS51, VPS52, VPS53, and mVPS54-V5-6His were kind gifts by from Juan Bonifacino and Chris Schindler (Perez-Victoria *et al.*, 2008, 2010b). To construct the corresponding expression plasmids, VAMP2, VAMP3, VAMP4, VAMP7, STX1A, and STX6 were PCR-amplified from a human brain cDNA library and GPR107 and GPR108 from HeLa and Hep3B cell cDNA libraries, respectively. The products were cloned into pME-Zeo plasmid digested with *Eco*RI and *Not*I. TMEM87A and TMEM87B cDNAs were amplified from HeLa and Hep3B cell cDNA libraries, respectively, and inserted into pME-Zeo. To construct the N-terminally HA-tagged expression plasmids, TMEM87A and TMEM87B, except for their signal sequences (ss), were PCR-amplified and the *Xho*I- and *Not*I-digested products cloned into pME-ssHA plasmid, which harbors an ss derived from human CD59 upstream of the HA tag. To construct C-terminally 3×HA-tagged expression plasmids, TMEM87A and TMEM87B, except for their stop codons, were PCR-amplified, and the products were cloned into *Xho*I- and *Mlu*I-digested pME-3xHA plasmid. To construct pLIB-BSD-VAMP4, pME-Zeo-VAMP4 was digested with *Eco*RI and *Not*I and cloned into pLIB-BSD digested with the same enzymes. Plasmid pLIB-BSD-ssHA-TMEM87A was constructed by PCR-amplifying a cDNA of ssHA-tagged TMEM87A, followed by digestion with *Sal*I and *Not*I and cloning into pLIB2-BSD. To construct pLIB-Hyg-RFP(S158T)-GPP34, pME-RFP(S158T)-GPP34 was digested with *Eco*RI and *Not*I and cloned into pLIB-Hyg.

Establishment of HAP1FF9, HEK293FF6, and HEK293TM10 cells

Retroviruses were produced in PLAT-GP packaging cells by cotransfection of the VSVG plasmid (pLC-VSVG) and pRetroX-Tet-On Advanced (Clontech) with pRetroX-VFG-GPI-Pur or pRetroX-FVG-TM-Pur. HAP1FF9 cells were established from HAP1 cells, kindly provided by Thijn R. Brummelkamp (Netherlands Cancer Institute, Amsterdam, Netherlands; Carette *et al.*, 2011b). HAP1 cells were infected with retroviruses bearing pRetroX-VFG-GPI-Pur and pRetroX-Tet-On Advanced, followed by selection with puromycin and G418. A HAP1FF9 cell clone was obtained after limiting dilution and karyotype analysis.

HEK293FF6 and HEK293TM10 cells were established from HEK293 cells by infection with retroviruses bearing pRetroX-Tet-On Advanced and pRetroX-VFG-GPI-Pur or pRetroX-FVG-TM-Pur, respectively, followed by selection with puromycin and G418 and limiting dilution.

Cell culture

HAP1-FF9 cells were cultured in Iscove's modified Dulbecco's medium supplemented with 10% fetal calf serum (FCS), 600 µg/ml G418, and 6 µg/ml puromycin. HEK293FF6, HEK293TM10, GARP-KO cell lines and TMEM87A and B double-KO (DKO) cell line established from HEK293FF6 were cultured in DMEM supplemented with 10% FCS, 600 µg/ml G418, and 1 µg/ml puromycin. V54KO cells stably expressing empty vector, mVPS54-V5-His, hVAMP4, or ssHA-hTMEM87A (V54KO+Vec, V54KO+VPS54, V54KO+VAMP4, and V54KO+TM87A, respectively) were cultured in DMEM supplemented with 10% FCS, 600 µg/ml G418, 1 µg/ml puromycin, and 10 µg/ml blasticidin. V54KO+Vec and V54KO+VPS54 stably expressing RFP(S158T)-GPP34 were cultured in DMEM supplemented with 10% FCS, 600 µg/ml G418, 1 µg/ml puromycin, 10 µg/ml blasticidin, and 500 µg/ml hygromycin B. RFP(S158T)-GPP34, a fusion protein of enhanced RFP and TGN protein GPP34, was used as a TGN marker (Shaner *et al.*, 2008).

Enrichment of transport-delayed HAP1FF9 mutant cells

A gene-trap virus was produced by transfection of PLAT-GP cells in eight 15-cm dishes using Lipofectamine 2000 and a mixture of pCMT-SApA-BSD and pLC-VSVG. The virus-containing supernatant was concentrated five times using PEG-it solution and then mixed with 8 µg/ml Polybrene. HAP1FF9 cells (6×10^7 cells in total) prepared in six-well plates containing 2.5×10^6 cells/well were infected by centrifugation at 2500 rpm for 2 h at 32°C. Two days after infection, the cells were selected with 6 µg/ml blasticidin for 1 wk. HAP1FF9 cells mutagenized by gene-trap vectors were cultured in medium containing 1 µg/ml Dox at 40°C for 24 h to induce and accumulate the VFG-GPI reporter protein in the ER (Maeda *et al.*, 2008; Fujita *et al.*, 2009). The cells were then quickly harvested with trypsin-EDTA and incubated in medium at 32°C for 60 min, followed by staining with an M2 anti-Flag antibody and PE-conjugated goat anti-mouse IgG. Cells with delayed surface expression of the reporter protein were enriched twice by cell sorting using a FACSAria (BD Bioscience, Franklin Lakes, NJ).

Sequence analysis of the gene-trap insertion sites

Genomic DNA was isolated from 3×10^7 cells using the Wizard Genomic DNA purification kit (Promega, Fitchburg, WI) according to the manufacturer's protocol. Genomic DNA (15 µg) was digested with *Hae*III, followed by ligation with the splinkerette adaptor (Horie *et al.*, 2011), which consists of two oligonucleotides: SpI-top-*Hae*III (CGAATCGTAACCGTTCGTACGAGAATTCGTACGAGAATCGCTGTCCTCTCCAACGAGCCAAGG) and SpIB-BLT-*Hae*III (CCTTGGCTCGTTTTTTTTTGCAAAAA). After ligation, the DNA fragments were digested with *Pvu*II, which cleaves the vector sequence between the 3′-long terminal repeat (LTR) and the upstream *Hae*III site, to prevent unwanted vector amplification. After column purification, the fragments were used as templates for splinkerette PCR using the SPI-P1 primer (CGAATCGTAACCGTTCGTACGAGAA) and the first LTR primer (AGTGTATGTAAACTTCTGACCCACTGG). The resulting DNA fragments were further amplified by nested PCRs using the SPI-P2 primer (TCGTACGAGAATCGCTGTCCTCTCC), the second LTR

primer (CTTGTGTCATGCACAAAGTAGATGTCC), Rd1Tru-LTR (ACACTCTTTCCCTACACGACGCTCTTCCGATCTGCTAGCTTGC CAAACCTACAGGTGGG), and Rd2Tru-Splink (GTGACTGGAG-TTCAGACGTGTGCTCTTCCGATCTGCTGTCCTCTCCAACGAG-CCAAGG). The underlined sequences indicate the Illumina sequencing primers. The resulting DNA products contained the end of the 5′LTR retroviral sequence, followed by the genomic DNA sequence flanking the insertion site ending at the *Hae*III restriction site and part of the splinkerette adaptor sequence. Illumina P5 (AATGATACGGCGACCACCG) and P7 (CAAGCAGAAGA-CGGCATACGA) adapters and barcode sequences were attached to the products by six cycles of PCR with 10 ng of each of initial PCR product as the template. Paired-end sequencing (151 base pairs × 2) was performed on the MiSeq (Illumina, San Diego, CA) system. The number of reads obtained from control and Sort 2 cells was ~1.4 million and 1.2 million, respectively.

Analysis of gene-trap insertions

FASTQ data files were analyzed using CLC Genomic Workbench software version 7.0.4 (CLC Bio) according to a previously described method (Carette *et al.*, 2011a,b). Briefly, after quality trimming and removal of the common LTR sequence, the 50–base pair reads were mapped onto the human genome (hg19). To exclude ambiguous alignments, mismatch reads were not allowed, and all nonspecific matched reads were ignored. To eliminate PCR amplification bias and determine the unique insertion sites, duplicate reads were removed and counted as one read (a unique insertion site). The independent insertion sites were further classified as being in the sense or antisense orientation compared with the gene. The total number of inactivating insertions, which consisted of all the sense or antisense orientations in the exons of the genes and the number of inactivating insertions per individual gene, were counted. The amount of enrichment of a particular gene in the screen was calculated by comparing the selected with the unselected population. For each gene, a *p* value and a *p* value corrected for the false-discovery rate (FDR) were calculated by the one-sided Fisher exact test using R software. A bubble plot was created using R software.

Establishment of knockout cell lines

GARP-KO cell lines and TM87A, B-DKO cell lines were generated using the CRISPR-Cas9 system. For the generation of GARP-KO cell lines, HEK293FF6 cells were transiently transfected with pX330 plasmids bearing the targeting sequence for VPS51 (GGGAGGCTCCGGAGCGTCGG), VPS52 (GGCCCGGGAACTG-GTGTTGC), VPS53 (GCTCACGCCCGAGGTGCAGC), and VPS54 (#1; GAGGCACTGGTGAAGAACTG and #2; GGACACACATCTG-GCAGTGA). After ~10 d of culture, cells with delayed VFG-GPI transport were sorted using a FACSAria cell sorter. The collected population was subjected to limiting dilution. To generate TM87A, B-DKO cell lines, HEK293FF6 cells were transiently transfected with pX330-mEGFP plasmids bearing the targeting sequence for hTMEM87A (GGAACAAACCTTACCTTTAT). After 3 d, cells with EGFP were sorted using a FACSAria cell sorter. The collected cells were subjected to limiting dilution. A clone that had no wild-type allele was picked up and used for next-round knockout process. A TMEM87A KO cell line was transiently transfected with pX330-mEGFP plasmids bearing the targeting sequence for hTMEM87B#1 or #2 (#1; GCCGCCGCTGCTTTCCCGCC, #2; GACCCCGGCGGCTGTGCGCG). After cell sorting, collected cells were subjected to limiting dilution. DNA sequences were analyzed by the Sanger method. The DNA sequence of each KO cell line is given in Supplemental Table S2.

Transport assay of reporter proteins using fluorescence-activated cell sorting

The transport assay was conducted as previously described (Maeda *et al.*, 2008; Fujita *et al.*, 2009). Briefly, cells were cultured in medium supplemented with 1 μg/ml Dox at 40°C for 24 h, harvested using trypsin-EDTA (Sigma-Aldrich), and then incubated in complete medium at 32°C for the required time. The cells were stained with an M2 anti-FLAG antibody and PE-conjugated goat anti-mouse IgG and then analyzed by FACSCantoII (BD). For the KD experiments, 0.5×10^6 cells were transfected with siRNA oligonucleotides purchased from Life Technologies using the Lipofectamine RNAi MAX reagent. Two days later, the cells were retransfected with the same siRNA oligos. On the next day, they were cultured in complete medium supplemented with 1 μg/ml Dox at 40°C for 24 h, after which transport was analyzed as described earlier. The siRNA sequences used were as follows: STX6#1, GCAACUGAAUUGAGUAU-AATT (siRNA ID s19959); STX6#2, GCAGUUAUGUUGGAAGAU-UTT (siRNA ID s19960); VAMP4#1, CAAACAACUUCGAAGGCAATT (siRNA ID s16525); and VAMP4#2, GAUUUGGACCUAGAAAU-GATT (siRNA ID s16526). For the transient expression of FVG-TM, 0.5×10^6 cells were transfected with pME-FLAG-VSVG^{full}-EGFP using the Lipofectamine 2000 reagent. On the next day, the incubation temperature was shifted to 40°C for 48 h. If required, expression plasmids alone or together with pME-FLAG-VSVG^{full}-EGFP were transfected into the cells described.

Western blotting

Cell lysate was prepared by incubation in buffer containing 50 mM Tris-HCl (pH 7.4), 150 mM NaCl, 1% Triton X-100, 5 mM EDTA, and 1× protease inhibitor cocktail (Roche, Basel, Switzerland), followed by centrifugation at 15,000 rpm for 15 min. Supernatant was recovered, mixed with SDS sample buffer, and boiled at 95°C for 5 min. Samples were run on 10–20% SDS–PAGE gels and transferred to polyvinylidene fluoride membranes. VPS52, VPS53, glyceraldehyde-3-phosphate dehydrogenase (GAPDH), STX6, and α-tubulin were detected by anti-VPS52, anti-VPS53, anti-GAPDH, anti-STX6, and anti–α-tubulin antibodies.

Quantitative reverse-transcription PCR

qRT-PCR was performed and normalized by HPRT1 expression as described previously (Theiler *et al.*, 2014).

Immunofluorescence microscopy

The cells were fixed with phosphate-buffered saline (PBS) containing 4% paraformaldehyde for 20 min at room temperature, followed by washing with 40 mM NH_4Cl for 10 min. The cells were double-stained with anti-TMEM87A or anti-HA7 and anti-GPP130 antibody followed by Alexa 488–conjugated anti-mouse goat secondary antibody and Alexa 594–conjugated anti-rabbit goat secondary antibody dissolved in staining buffer A (PBS containing 1% bovine serum albumin [BSA], 0.1% NaN_3, and 0.1% Triton X-100). For intracellular localization of CD59, cells were pretreated with 1 unit/ml PI-PLC (Life Technologies) for 1.5 h at 37°C. The cells were double-stained with anti-CD59 and anti-LAMP1 or anti-EEA1 as primary antibodies followed by secondary antibodies as described in staining buffer B (PBS containing 1% BSA, 0.1% NaN_3, and 0.1% saponin). Confocal images were acquired on a FluoView FV1000 (Olympus, Tokyo, Japan).

Flow cytometric analysis of surface expression of CD59

Surface expression of CD59 was determined as previously described (Hirata *et al.*, 2013).

Transport assay of reporter proteins based on immunofluorescence microscopy analysis

Cells stably expressing RFP(S158T)-GPP34 were cultured in medium supplemented with 1 μg/ml Dox at 40°C for 24 h. On the next day, they were washed with cold PBS and chased with warmed complete medium at 32°C containing 100 μg/ml cycloheximide (CHX) for the indicated time, followed by fixation. For post-Golgi anterograde transport analysis, the cells were precultured at 19°C for 3 h with complete medium containing 100 μg/ml CHX and then chased at 32°C. After fixation, the cells were stained with M2 anti-FLAG antibody as the primary antibody and Alexa 647–conjugated anti-mouse goat as the secondary antibody; the antibodies were dissolved in staining buffer without detergent. Images were obtained as described.

Retrograde transport assay of CTxB

The cells were washed twice with PBS and then cultured in cold medium supplemented with 10 mM 4-(2-hydroxyethyl)-1-piperazineethanesulfonic acid and 1 μg/ml CTxB-Alexa 488 for 30 min on ice. After incubation, the cells were washed with ice-cold PBS once and incubated in warmed complete medium at 37°C for 60 min, followed by fixation and staining with combinations of anti-golgin97 antibody as primary antibody and Alexa 594–conjugated anti-mouse goat secondary antibody dissolved in staining buffer A. Images were obtained as described.

Quantification of immunofluorescence images

Fluorescence intensities were quantified using MetaMorph 3.0 (Molecular Devices, Sunnyvale, CA). The VFG-GPI, CD59, and CTxB regions and the TGN (RFP-GPP34– or golgin97-positive regions), cell surface (FLAG-positive regions), and lysosomes (LAMP1 positive regions) in each fluorescence image were assigned a threshold by MetaMorph 3.0. The fluorescence intensities of total VFG-GPI, CD59, and CTxB ($I_{(t)}$) and of VFG-GPI, CD59, and CTxB that colocalized with markers ($I_{(m)}$) were measured, and their ratios were expressed as the percentage of $I_{(m)}$ in $I_{(t)}$. Means and standard errors were calculated and plotted from 10 independent fluorescence images.

Expression cloning

A retrovirus-based cDNA library from human brain was stably transfected into V54KO cells. Those cells with increased transport were sorted using a cell sorter. The culture and sorting steps were repeated once more. Genomic DNA was isolated from pre-enrichment control cells and the sorted cells as described earlier. Genomic DNA (15 μg) was digested with Covaris S2 (M&S, Osaka, Japan) using the 800–base pair protocol, followed by repair of the ends of the products and ligation with the aforementioned splinkerette adaptor. After ligation, the DNA fragments were used as templates for splinkerette PCR using the primers SPI-P2 and pLIB-F0 (CTCCCTTTATCCAGCCCTCACTCC). The resulting DNA fragments were further amplified by nested PCRs using Rd1Tru-pLIB (ACACTCTTTCCCTACACGACGCTCTTCCGATCTCGCCGGAATTCGTTAGGCCATTA) and Rd2Tru-Splink (GTGACTGGAGTTCAGACGTGTGCTCTTCCGATCTGCTGTCCTCTCCAACGAGCCAAGG). The underlined sequences indicate the Illumina sequencing primers. Illumina P5 and P7 adapters and barcode sequences were attached as described, and single-end sequencing (151 base pairs) was performed on the HiSeq2500 (Illumina) system. The number of reads obtained from control and sorted cells was ~26 million and 7.2 million, respectively.

Sequence analysis of recovered cDNAs

FASTQ data files were analyzed using CLC Genomic Workbench software, version 7.0.4. After quality trimming and removal of the common pLIB sequence, the reads were mapped to the human genome (hg19). For each gene, test statistics, a p value, and the p value corrected for the FDR of Kal's Z test were calculated by comparing the number of mapped reads using CLC Genomic Workbench software, version 7.0.4 (Kal *et al.*, 1999). Supplemental Table S3 lists the highest to lowest test statistics of Kal's Z test.

ACKNOWLEDGMENTS

We thank T. R. Brummelkamp and the Whitehead Institute for Biomedical Research for HAP1 cells; K. Horie for pCMT-SAhygpA-NP21; C. Schindler and J. S. Bonifacino for rabbit polyclonal anti-VPS52 and anti-VPS53 and expression plasmids of VPS51, VPS52, VPS53, and VPS54; Noriyuki Kanzawa, Romina Theiler, Gun-Hee Lee, and Jihyoun Seong for helpful discussions; Keiko Kinoshita, Yukari Onoe, and Kana Miyanagi for technical help; and Kohjiro Nakamura and Yuko Kabumoto for assistance with cell sorting. This work was supported by grant-in-aids from the Ministry of Education, Culture, Sports, Science and Technology of Japan (to T.K. and M.F.), the National Natural Science Foundation for Young Scientists of China (31400693), and the Natural Science Foundation of Jiangsu Province (BK20140141) (to M.F.). T.H. was supported by the Japan Society for the Promotion of Science Research Fellowship.

REFERENCES

Belenkaya TY, Wu Y, Tang X, Zhou B, Cheng L, Sharma YV, Yan D, Selva EM, Lin X (2008). The retromer complex influences Wnt secretion by recycling wntless from endosomes to the trans-Golgi network. Dev Cell 14, 120–131.

Bonifacino JS, Glick BS (2004). The mechanisms of vesicle budding and fusion. Cell 116, 153–166.

Bonifacino JS, Hierro A (2011). Transport according to GARP: receiving retrograde cargo at the trans-Golgi network. Trends Cell Biol 21, 159–167.

Brandizzi F, Barlowe C (2013). Organization of the ER-Golgi interface for membrane traffic control. Nat Rev Mol Cell Biol 14, 382–392.

Brunet S, Sacher M (2014). In sickness and in health: the role of TRAPP and associated proteins in disease. Traffic 15, 803–818.

Calakos N, Bennett MK, Peterson KE, Scheller RH (1994). Protein-protein interactions contributing to the specificity of intracellular vesicular trafficking. Science 263, 1146–1149.

Carette JE, Guimaraes CP, Wuethrich I, Blomen VA, Varadarajan M, Sun C, Bell G, Yuan B, Muellner MK, Nijman SM, *et al.* (2011a). Global gene disruption in human cells to assign genes to phenotypes by deep sequencing. Nat Biotechnol 29, 542–546.

Carette JE, Raaben M, Wong AC, Herbert AS, Obernosterer G, Mulherkar N, Kuehne AI, Kranzusch PJ, Griffin AM, Ruthel G, *et al.* (2011b). Ebola virus entry requires the cholesterol transporter Niemann-Pick C1. Nature 477, 340–343.

Chen YA, Scheller RH (2001). SNARE-mediated membrane fusion. Nat Rev Mol Cell Biol 2, 98–106.

Chia PZ, Gunn P, Gleeson PA (2013). Cargo trafficking between endosomes and the trans-Golgi network. Histochem Cell Biol 140, 307–315.

Choudhury A, Marks DL, Proctor KM, Gould GW, Pagano RE (2006). Regulation of caveolar endocytosis by syntaxin 6-dependent delivery of membrane components to the cell surface. Nat Cell Biol 8, 317–328.

Cong L, Ran FA, Cox D, Lin S, Barretto R, Habib N, Hsu PD, Wu X, Jiang W, Marraffini LA, Zhang F (2013). Multiplex genome engineering using CRISPR/Cas systems. Science 339, 819–823.

Conibear E, Stevens TH (2000). Vps52p, Vps53p, and Vps54p form a novel multisubunit complex required for protein sorting at the yeast late Golgi. Mol Biol Cell 11, 305–323.

Elling U, Taubenschmid J, Wirnsberger G, O'Malley R, Demers SP, Vanhaelen Q, Shukalyuk AI, Schmauss G, Schramek D, Schnuetgen F, *et al.* (2011). Forward and reverse genetics through derivation of haploid mouse embryonic stem cells. Cell Stem Cell 9, 563–574.

Feinstein M, Flusser H, Lerman-Sagie T, Ben-Zeev B, Lev D, Agamy O, Cohen I, Kadir R, Sivan S, Leshinsky-Silver E, *et al.* (2014). VPS53 mutations cause progressive cerebello-cerebral atrophy type 2 (PCCA2). J Med Genet 51, 303–308.

Franch-Marro X, Wendler F, Guidato S, Griffith J, Baena-Lopez A, Itasaki N, Maurice MM, Vincent JP (2008). Wingless secretion requires

endosome-to-Golgi retrieval of Wntless/Evi/Sprinter by the retromer complex. Nat Cell Biol 10, 170–177.
Fujita M, Maeda Y, Ra M, Yamaguchi Y, Taguchi R, Kinoshita T (2009). GPI glycan remodeling by PGAP5 regulates transport of GPI-anchored proteins from the ER to the Golgi. Cell 139, 352–365.
Fujita M, Watanabe R, Jaensch N, Romanova-Michaelides M, Satoh T, Kato M, Riezman H, Yamaguchi Y, Maeda Y, Kinoshita T (2011). Sorting of GPI-anchored proteins into ER exit sites by p24 proteins is dependent on remodeled GPI. J Cell Biol 194, 61–75.
Ganley IG, Espinosa E, Pfeffer SR (2008). A syntaxin 10-SNARE complex distinguishes two distinct transport routes from endosomes to the trans-Golgi in human cells. J Cell Biol 180, 159–172.
Harterink M, Port F, Lorenowicz MJ, McGough IJ, Silhankova M, Betist MC, van Weering JR, van Heesbeen RG, Middelkoop TC, Basler K, *et al.* (2011). A SNX3-dependent retromer pathway mediates retrograde transport of the Wnt sorting receptor Wntless and is required for Wnt secretion. Nat Cell Biol 13, 914–923.
Hirata T, Fujita M, Kanzawa N, Murakami Y, Maeda Y, Kinoshita T (2013). Glycosylphosphatidylinositol mannosyltransferase II is the rate-limiting enzyme in glycosylphosphatidylinositol biosynthesis under limited dolichol-phosphate mannose availability. J Biochem 154, 257–264.
Hong W, Lev S (2013). Tethering the assembly of SNARE complexes. Trends Cell Biol 24, 35–43.
Horie K, Kokubu C, Yoshida J, Akagi K, Isotani A, Oshitani A, Yusa K, Ikeda R, Huang Y, Bradley A, Takeda J (2011). A homozygous mutant embryonic stem cell bank applicable for phenotype-driven genetic screening. Nat Methods 8, 1071–1077.
Inadome H, Noda Y, Adachi H, Yoda K (2005). Immunoisolaton of the yeast Golgi subcompartments and characterization of a novel membrane protein, Svp26, discovered in the Sed5-containing compartments. Mol Cell Biol 25, 7696–7710.
Irannejad R, Wedegaertner PB (2010). Regulation of constitutive cargo transport from the trans-Golgi network to plasma membrane by Golgi-localized G protein betagamma subunits. J Biol Chem 285, 32393–32404.
Kal AJ, van Zonneveld AJ, Benes V, van den Berg M, Koerkamp MG, Albermann K, Strack N, Ruijter JM, Richter A, Dujon B, *et al.* (1999). Dynamics of gene expression revealed by comparison of serial analysis of gene expression transcript profiles from yeast grown on two different carbon sources. Mol Biol Cell 10, 1859–1872.
Karlsson P, Droce A, Moser JM, Cuhlmann S, Padilla CO, Heimann P, Bartsch JW, Fuchtbauer A, Fuchtbauer EM, Schmitt-John T (2013). Loss of vps54 function leads to vesicle traffic impairment, protein mis-sorting and embryonic lethality. Int J Mol Sci 14, 10908–10925.
Kinoshita T, Fujita M, Maeda Y (2008). Biosynthesis, remodelling and functions of mammalian GPI-anchored proteins: recent progress. J Biochem 144, 287–294.
Laufman O, Hong W, Lev S (2011). The COG complex interacts directly with Syntaxin 6 and positively regulates endosome-to-TGN retrograde transport. J Cell Biol 194, 459–472.
Maeda Y, Ide T, Koike M, Uchiyama Y, Kinoshita T (2008). GPHR is a novel anion channel critical for acidification and functions of the Golgi apparatus. Nat Cell Biol 10, 1135–1145.
Mali P, Yang L, Esvelt KM, Aach J, Guell M, DiCarlo JE, Norville JE, Church GM (2013). RNA-guided human genome engineering via Cas9. Science 339, 823–826.
Mallard F, Antony C, Tenza D, Salamero J, Goud B, Johannes L (1998). Direct pathway from early/recycling endosomes to the Golgi apparatus revealed through the study of shiga toxin B-fragment transport. J Cell Biol 143, 973–990.
Mallard F, Tang BL, Galli T, Tenza D, Saint-Pol A, Yue X, Antony C, Hong W, Goud B, Johannes L (2002). Early/recycling endosomes-to-TGN transport involves two SNARE complexes and a Rab6 isoform. J Cell Biol 156, 653–664.
Maruyama H, Morino H, Ito H, Izumi Y, Kato H, Watanabe Y, Kinoshita Y, Kamada M, Nodera H, Suzuki H, *et al.* (2010). Mutations of optineurin in amyotrophic lateral sclerosis. Nature 465, 223–226.
Moser JM, Bigini P, Schmitt-John T (2013). The wobbler mouse, an ALS animal model. Mol Genet Genomics 288, 207–229.
Nishimoto-Morita K, Shin HW, Mitsuhashi H, Kitamura M, Zhang Q, Johannes L, Nakayama K (2009). Differential effects of depletion of ARL1 and ARFRP1 on membrane trafficking between the trans-Golgi network and endosomes. J Biol Chem 284, 10583–10592.
Novarino G, Fenstermaker AG, Zaki MS, Hofree M, Silhavy JL, Heiberg AD, Abdellateef M, Rosti B, Scott E, Mansour L, *et al.* (2014). Exome sequencing links corticospinal motor neuron disease to common neurodegenerative disorders. Science 343, 506–511.
Oka T, Ungar D, Hughson FM, Krieger M (2004). The COG and COPI complexes interact to control the abundance of GEARs, a subset of Golgi integral membrane proteins. Mol Biol Cell 15, 2423–2435.
Olson AL, Knight JB, Pessin JE (1997). Syntaxin 4, VAMP2, and/or VAMP3/cellubrevin are functional target membrane and vesicle SNAP receptors for insulin-stimulated GLUT4 translocation in adipocytes. Mol Cell Biol 17, 2425–2435.
Pepperkok R, Scheel J, Horstmann H, Hauri HP, Griffiths G, Kreis TE (1993). Beta-COP is essential for biosynthetic membrane transport from the endoplasmic reticulum to the Golgi complex in vivo. Cell 74, 71–82.
Perez-Victoria FJ, Abascal-Palacios G, Tascon I, Kajava A, Magadan JG, Pioro EP, Bonifacino JS, Hierro A (2010a). Structural basis for the wobbler mouse neurodegenerative disorder caused by mutation in the Vps54 subunit of the GARP complex. Proc Natl Acad Sci USA 107, 12860–12865.
Perez-Victoria FJ, Bonifacino JS (2009). Dual roles of the mammalian GARP complex in tethering and SNARE complex assembly at the trans-golgi network. Mol Cell Biol 29, 5251–5263.
Perez-Victoria FJ, Mardones GA, Bonifacino JS (2008). Requirement of the human GARP complex for mannose 6-phosphate-receptor-dependent sorting of cathepsin D to lysosomes. Mol Biol Cell 19, 2350–2362.
Perez-Victoria FJ, Schindler C, Magadan JG, Mardones GA, Delevoye C, Romao M, Raposo G, Bonifacino JS (2010b). Ang2/fat-free is a conserved subunit of the Golgi-associated retrograde protein complex. Mol Biol Cell 21, 3386–3395.
Peter F, Plutner H, Zhu H, Kreis TE, Balch WE (1993). Beta-COP is essential for transport of protein from the endoplasmic reticulum to the Golgi in vitro. J Cell Biol 122, 1155–1167.
Schindler C, Chen Y, Pu J, Guo X, Bonifacino JS (2015). EARP is a multisubunit tethering complex involved in endocytic recycling. Nat Cell Biol 17, 639–650.
Schmitt-John T, Drepper C, Mussmann A, Hahn P, Kuhlmann M, Thiel C, Hafner M, Lengeling A, Heimann P, Jones JM, *et al.* (2005). Mutation of Vps54 causes motor neuron disease and defective spermiogenesis in the wobbler mouse. Nat Genet 37, 1213–1215.
Shaner NC, Lin MZ, McKeown MR, Steinbach PA, Hazelwood KL, Davidson MW, Tsien RY (2008). Improving the photostability of bright monomeric orange and red fluorescent proteins. Nat Methods 5, 545–551.
Shitara A, Shibui T, Okayama M, Arakawa T, Mizoguchi I, Sakakura Y, Takuma T (2013). VAMP4 is required to maintain the ribbon structure of the Golgi apparatus. Mol Cell Biochem 380, 11–21.
Siniossoglou S, Pelham HR (2002). Vps51p links the VFT complex to the SNARE Tlg1p. J Biol Chem 277, 48318–48324.
Stow JL, de Almeida JB, Narula N, Holtzman EJ, Ercolani L, Ausiello DA (1991). A heterotrimeric G protein, G alpha i-3, on Golgi membranes regulates the secretion of a heparan sulfate proteoglycan in LLC-PK1 epithelial cells. J Cell Biol 114, 1113–1124.
Tafesse FG, Guimaraes CP, Maruyama T, Carette JE, Lory S, Brummelkamp TR, Ploegh HL (2014). GPR107, a G-protein-coupled receptor essential for intoxication by Pseudomonas aeruginosa exotoxin A, localizes to the Golgi and is cleaved by furin. J Biol Chem 289, 24005–24018.
Tai G, Lu L, Wang TL, Tang BL, Goud B, Johannes L, Hong W (2004). Participation of the syntaxin 5/Ykt6/GS28/GS15 SNARE complex in transport from the early/recycling endosome to the trans-Golgi network. Mol Biol Cell 15, 4011–4022.
Tanaka S, Maeda Y, Tashima Y, Kinoshita T (2004). Inositol deacylation of glycosylphosphatidylinositol-anchored proteins is mediated by mammalian PGAP1 and yeast Bst1p. J Biol Chem 279, 14256–14263.
Tashima Y, Taguchi R, Murata C, Ashida H, Kinoshita T, Maeda Y (2006). PGAP2 is essential for correct processing and stable expression of GPI-anchored proteins. Mol Biol Cell 17, 1410–1420.
Theiler R, Fujita M, Nagae M, Yamaguchi Y, Maeda Y, Kinoshita T (2014). The alpha-helical region in p24gamma2 subunit of p24 protein cargo receptor is pivotal for the recognition and transport of glycosylphosphatidylinositol-anchored proteins. J Biol Chem 289, 16835–16843.
Ungar D, Oka T, Krieger M, Hughson FM (2006). Retrograde transport on the COG railway. Trends Cell Biol 16, 113–120.
VanRheenen SM, Cao X, Lupashin VV, Barlowe C, Waters MG (1998). Sec35p, a novel peripheral membrane protein, is required for ER to Golgi vesicle docking. J Cell Biol 141, 1107–1119.
Wiederkehr A, De Craene JO, Ferro-Novick S, Novick P (2004). Functional specialization within a vesicle tethering complex: bypass of a subset of exocyst deletion mutants by Sec1p or Sec4p. J Cell Biol 167, 875–887.
Zhou GL, Na SY, Niedra R, Seed B (2014). Deficits in receptor-mediated endocytosis and recycling in cells from mice with Gpr107 locus disruption. J Cell Sci 127, 3916–3927.

Human Molecular Genetics, 2015, 1–14

doi: 10.1093/hmg/ddv331
Original Article

ORIGINAL ARTICLE

Mutations in *PIGY*: expanding the phenotype of inherited glycosylphosphatidylinositol deficiencies

Biljana Ilkovski[1,†], Alistair T. Pagnamenta[3,†], Gina L. O'Grady[1,5], Taroh Kinoshita[6], Malcolm F. Howard[3], Monkol Lek[7,8], Brett Thomas[7,8], Anne Turner[9], John Christodoulou[2,10], David Sillence[2,10], Samantha J.L. Knight[3], Niko Popitsch[3], David A. Keays[11], Consuelo Anzilotti[4], Anne Goriely[12], Leigh B. Waddell[1,5], Fabienne Brilot[1,5], Kathryn N. North[1,5,13], Noriyuki Kanzawa[6], Daniel G. Macarthur[7,8], Jenny C. Taylor[3], Usha Kini[14,*], Yoshiko Murakami[6] and Nigel F. Clarke[1,5,*]

[1]Institute for Neuroscience and Muscle Research, [2]Western Sydney Genetics Program, Children's Hospital at Westmead, Westmead, NSW, Australia, [3]National Institute for Health Research Biomedical Research Centre, Wellcome Trust Centre for Human Genetics, University of Oxford, [4]The Henry Wellcome Building for Molecular Physiology, University of Oxford, Oxford OX3 7BN, UK, [5]Discipline of Paediatrics and Child Health, University of Sydney, Sydney, NSW, Australia, [6]Department of Immunoregulation, Research Institute for Microbial Diseases, and WPI Immunology Frontier Research Center, Osaka University, 3-1 Yamadaoka, Suita, Osaka 565-0871, Japan, [7]Analytic and Translational Genetics Unit, Massachusetts General Hospital, Boston, MA, USA, [8]Broad Institute of Harvard and Massachusetts Institute of Technology, Cambridge, MA, USA, [9]Department of Clinical Genetics, Sydney Children's Hospital, Sydney, NSW, Australia, [10]Discipline of Genetic Medicine, Children's Hospital at Westmead Clinical School, Sydney, NSW, Australia, [11]Institute of Molecular Pathology, Vienna 1030, Austria, [12]Weatherall Institute of Molecular Medicine, University of Oxford, Oxford OX3 9DS, UK, [13]Murdoch Children's Research Institute, The Royal Children's Hospital, Flemington Road, Parkville, VIC, Australia and [14]Department of Clinical Genetics, Oxford University Hospitals NHS Trust, Oxford OX3 9DU, UK

*To whom correspondence should be addressed at: Institute for Neuroscience and Muscle Research, The Children's Hospital at Westmead, Locked Bag 4001, Westmead, NSW 2145, Australia. Tel: +61 298451453; Fax: +61 298453078; Email: nigel.clarke@health.nsw.gov.au (N.F.C.); Department of Clinical Genetics, Oxford University Hospitals NHS Trust, Oxford OX3 9DU, UK. Tel: +44 1865 226020; Fax: +44 1865 223572; Email: Usha.Kini@ouh.nhs.uk (U.K.)

Abstract

Glycosylphosphatidylinositol (GPI)-anchored proteins are ubiquitously expressed in the human body and are important for various functions at the cell surface. Mutations in many GPI biosynthesis genes have been described to date in patients with multi-system disease and together these constitute a subtype of congenital disorders of glycosylation. We used whole exome

†The authors wish it to be known that, in their opinion, the first two authors, Biljana Ilkovski and Alistair Pagnamenta should be regarded as joint First Authors.
Received: May 17, 2015. **Revised:** July 21, 2015. **Accepted:** August 10, 2015

sequencing in two families to investigate the genetic basis of disease and used RNA and cellular studies to investigate the functional consequences of sequence variants in the *PIGY* gene. Two families with different phenotypes had homozygous recessive sequence variants in the GPI biosynthesis gene *PIGY*. Two sisters with c.137T>C (p.Leu46Pro) *PIGY* variants had multi-system disease including dysmorphism, seizures, severe developmental delay, cataracts and early death. There were significantly reduced levels of GPI-anchored proteins (CD55 and CD59) on the surface of patient-derived skin fibroblasts (~20–50% compared with controls). In a second, consanguineous family, two siblings had moderate development delay and microcephaly. A homozygous *PIGY* promoter variant (c.-540G>A) was detected within a 7.7 Mb region of autozygosity. This variant was predicted to disrupt a SP1 consensus binding site and was shown to be associated with reduced gene expression. Mutations in *PIGY* can occur in coding and non-coding regions of the gene and cause variable phenotypes. This article contributes to understanding of the range of disease phenotypes and disease genes associated with deficiencies of the GPI-anchor biosynthesis pathway and also serves to highlight the potential importance of analysing variants detected in 5′-UTR regions despite their typically low coverage in exome data.

Introduction

Glycosylphosphatidylinositol (GPI) acts as a membrane anchor for many cell-surface proteins including receptors, enzymes and adhesion molecules. At least 25 genes are involved in the step-wise production of mature GPI-anchored proteins (GPI-APs) (1). GPI biosynthesis is initiated in the endoplasmic reticulum from phosphatidylinositol (PI) in a reaction mediated by the GPI-*N*-acetylglucosaminyltransferase (GPI-GnT) complex. The GPI-GnT enzyme complex consists of seven proteins including PIG-A, PIG-C, PIG-H, PIG-P, PIG-Q, DPM2 and PIG-Y. Phosphatidylinositol glycan class Y (PIG-Y), the smallest subunit of this complex, is a 71-amino acid protein containing two putative transmembrane domains and it directly associates with the catalytic subunit PIG-A. In the absence of PIG-Y activity, the cell surface levels of GPI-APs are severely decreased (2).

The first disorders to be described in association with deficiencies of the GPI-anchor biosynthesis pathway were paroxysmal nocturnal haemoglobinuria (PNH), caused by somatic mutations in PIGA (3), in haemopoietic cells, and inherited GPI deficiency caused by a hypomorphic promoter mutation in PIGM (4). Whole exome sequencing (WES) technology has facilitated the discovery of pathogenic mutations in several other GPI biosynthesis genes. Germline mutations in PIGL (5), *PIGM* (4), *PIGN* (6), PIGO (7), PIGT (8), PIGV (9), *PIGW* (10), PIGQ (11) and PIGA (12) have all been reported in a small number of families in association with multi-system disease. Common clinical features include moderate to severe developmental delay, seizures and dysmorphic facial features. Reduced levels of GPI-APs CD59, or membrane attack complex-inhibitory protein, and FLAER (fluorescently labelled inactive toxin aerolysin which binds to GPI-linked structures) at the cell surface have been described in many of these patients (13).

We have identified two different sequence variants in *PIGY* in two unrelated families associated with different phenotypes. In Family A, we identified a homozygous c.137T>C variant in two affected sisters presenting with a multi-system disease encompassing dysmorphism, developmental delay, seizures, cataracts and gastrointestinal dysmotility. Levels of two GPI-APs on patient fibroblasts were reduced, providing evidence that these sequence variants impair GPI synthesis and are pathogenic. In Family B, we identified a c.-540G>A mutation in the promoter region in a consensus SP1 site. The affected siblings from Family B have primary microcephaly, moderate developmental delay and are more mildly affected in comparison to Family A. This report identifies *PIGY* as a new disease-causing gene with variable expressivity and increases our knowledge of the phenotypes that can arise from abnormal GPI biosynthesis.

Results

Clinical descriptions

Family A

Two affected sisters were the only children of a non-consanguineous Australian couple of Caucasian decent. Patient II-1 from Family A was born at 32 weeks gestation and had a complicated course with necrotizing enterocolitis and chronic lung disease. She was dysmorphic and had brachyphalangy (Fig. 1), 2–3 toe syndactyly, elbow and knee flexion contractures and severe bilateral hip dysplasia. At 5 months of age, she developed an intractable seizure disorder with multifocal spike and slow wave activity on EEG. This was followed by developmental regression and death at 2 years of age from a respiratory infection.

II-2 had abnormal antenatal scans from 25 weeks gestation with enlarged echogenic kidneys and bowel and long-bone growth failure. Delivery was induced at 28 weeks gestation due to polyhydramnios. Similar dysmorphic features, brachyphalangy, proximal limb shortening, contractures and left hip dysplasia were present. She had bilateral inguinal hernias and bilateral dilatation of the renal collecting systems, with markedly increased echogenicity of the renal parenchyma. Intractable seizures commenced at 6 weeks of age, her development regressed and at 5 months she was mostly unresponsive with poor vision. She died at 7 months of age secondary to an aspiration.

In addition, both affected sisters from Family A had congenital cataracts, intermittent episodes of abdominal distress and vomiting and growth failure. Head growth was normal. MRI brain was normal in both neonates, but showed loss of white matter and cerebral volume in Patient II-1 at 9 months. No abnormalities were present on diffusion-weighted images. Skeletal survey showed osteopenia and brachytelephalangy. Creatine kinase (CK) measurements were persistently elevated in both siblings (554–3640 U/l, normal range = 15–180 U/l). Muscle biopsies were taken from rectus abdominus (II-1, 9 months) and vastus lateralis (II-2, 8 days) showed moderate variation in fibre size with many small, rounded atrophic fibres, increased fibrosis and adipose tissue. No degenerating or regenerating fibres were seen, but in Patient II-2, acid phosphatase staining was increased suggestive of active degeneration.

Alkaline phosphatase levels were elevated in both patients (443–853 u/l, normal range = 40–300 U/l). Extensive metabolic work-up was normal including urine metabolic and oligosaccharide screen, lactate, thyroid function, very long

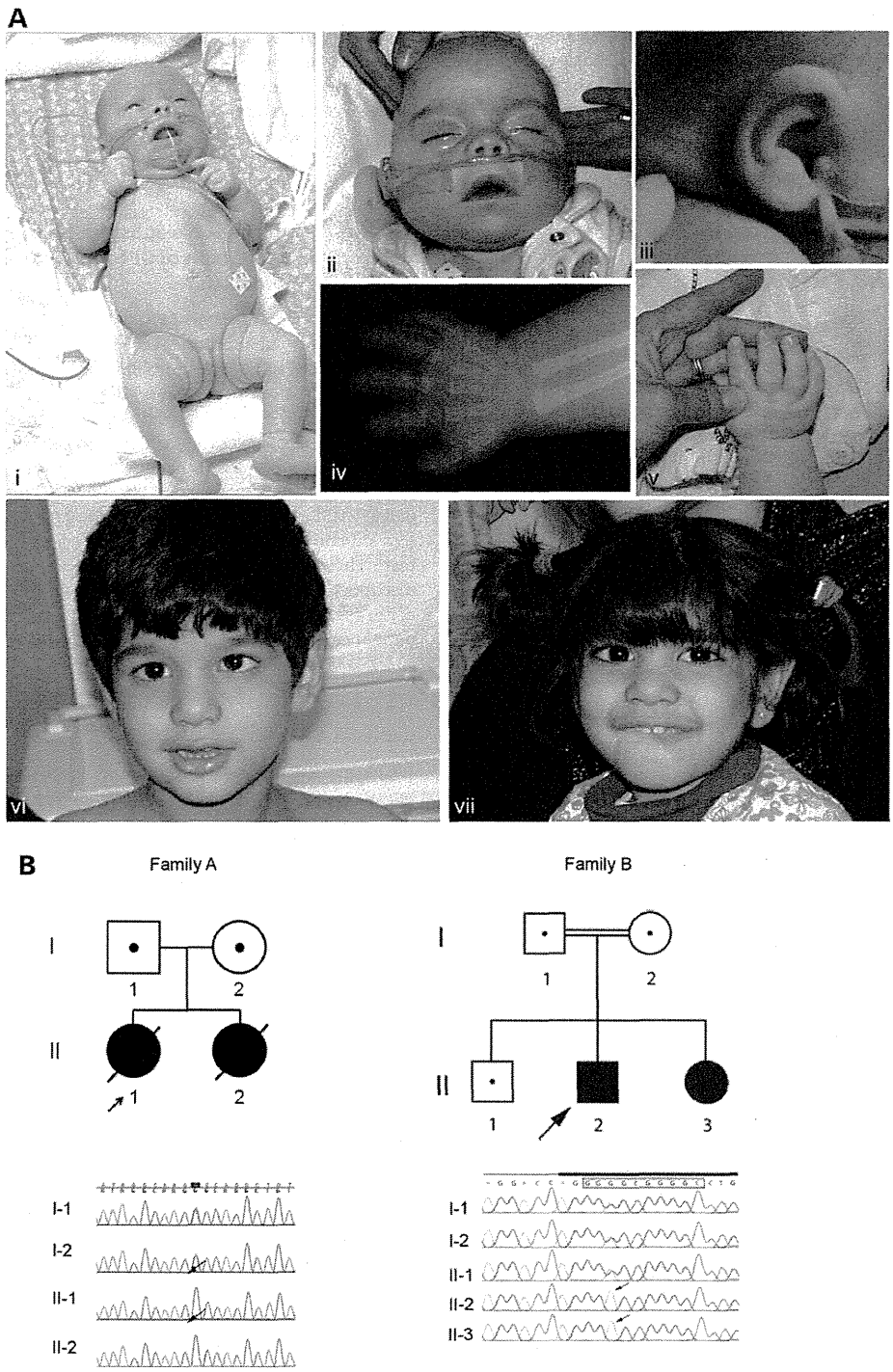

Figure 1. (A) Clinical features of patients with mutations in PIGY. Family A, Patient II-1 had proximal limb shortening, left hip dysplasia and contractures were present at the elbows, hips and knees (i). Dysmorphic features included bitemporal narrowing, upturned nares, depressed nasal bridge, deep-set eyes, a short neck (ii) and ears with thickened helices and fleshy earlobes (iii). Brachyphalange, fifth finger clinodactyly and adducted thumbs were present (v). Brachytelephalange was present on X-ray (iv). Family B Patient II-2 (v) and Patient II-3 (vi) had a milder phenotype, with soft dysmorphic features including long palpebral fissures, a bulbous tip to the nose and a wide mouth. Patient II-2 had a strabismus. (B) Pedigrees of Families A and B. Shading indicates affected individuals. The probands are indicated with an arrow. Proven heterozygote carriers are shown by a dot. Sanger sequencing validation from Family A confirms the homozygous missense variant c.137T>C (p.Leu46Pro) in the *PIGY* gene (NM_001042616.1) in the two affected sisters. Region shown corresponds to chr4: 89,442,795–813 (hg19). For Family B, Sanger validation and segregation testing of the *PIGY* promoter variant c.-540G>A is shown. The consensus SP1 binding motif is indicated with a black rectangle. Region shown corresponds to chr4: 89,444,938–958.

chain fatty acids, 7-dehydrocholesterol, 8-dehydrocholesterol and 8(9) cholestanol, serum transferrin isoforms, white blood cell enzyme testing for CDG type 1A and 1B, white blood cell lysosomal enzymes, bile alcohol analysis, sterol analysis, urine and plasma creatine and guanidine-acetate and CSF lactate, amino acids and neurotransmitters. Neuraminidase on cultured skin fibroblasts were normal. Respiratory chain enzymology was normal in liver. Complex 1-IV were all low relative to protein in muscle, but citrate synthase was also low likely secondary to poor handling and storage. Karyotype was also normal. Additional studies in II-2 included mildly elevated erythrocyte plasmalogen levels and normal serum phytanic acid, normal DHAP-AT and DHAP-s enzyme activity and subtelomere FISH.

Family B

Two siblings, born to consanguineous parents of Pakistani descent, were referred with global developmental delay and microcephaly. II-2 was born following an uncomplicated pregnancy and delivery, but had microcephaly at 6 weeks of age. At 5 years this was 46 cm (−3 to −4 SD). His developmental milestones were delayed. He sat with support at 15 months and walked at 3 years of age. His speech was delayed with the acquisition of only short two to three word sentences at the age of 5 years. He was short-sighted with a strabismus and had behavioural difficulties with aggressive outbursts.

II-3 was born following an uncomplicated pregnancy and delivery. She had microcephaly noted at 2 weeks of age and at 2 years had a head circumference of 42.1 cm (−4 to −5SD). Her development was delayed. She sat with support at 18 months and was not walking at the age of 3 years. Her speech was better than her brother's with 10–15 single words at age 3 years. She had poor concentration and was hyperactive.

The parental head circumferences were within the normal range. Neither child had seizures. There was mild facial dysmorphism with long palpebral fissures, a bulbous tip to the nose and a wide mouth (Fig. 1A). Brachytelephalangy was not present.

Genetic analysis

WES of DNA from II-1 and II-2 from Family A identified a homozygous missense variant c.137T>C (p.Leu46Pro) in the coding region of the *PIGY* gene in both individuals (NM_001042616.1). Sanger sequencing confirmed variant segregation was consistent with an autosomal recessive inheritance pattern (Fig. 1C). Analysis of allelic ratios across chromosome 4 indicated that the homozygous c.137T>C variant lay within a ~10 Mb segment of autozygosity, suggesting that the parents may be distantly related (Supplementary Material, Fig. S1). *In silico* analysis predicted the variant to be pathogenic (*PolyPhen-2 score of 1.0*) (14) and the variant was not present in the NHLBI Exome Variant Server (http://evs.gs.washington.edu/EVS/, accessed April 2014), 63 000 exomes ExAc (Exome Aggregation Consortium (ExAC), Cambridge, MA, URL: http://exac.broadinstitute.org/, accessed, January 2015) or in the 1000 genomes project (15,16).

For Family B, an autozygosity mapping approach identified candidate regions on 4q22.1-q22.3 and 10p14-pter, both 7.7 Mb in size. WES was performed for the proband (II-2), and the resulting variants were intersected with these two candidate loci. This revealed a c.-540G>A variant in a conserved region of the *PIGY* 5′-UTR. This variant was not in either of the publically available databases mentioned above and was not detected in 274 in-house genomes of mixed ancestry (see www.well.ox.ac.uk/wgs500) or 108 Punjabi individuals from Lahore. However, it should be noted that the region of the variant in Family B is not covered well by either the SureSelect or TrueSeq platforms (Supplementary Material, Fig. S2) and is not covered in the ExAC dataset. Sanger sequencing confirmed segregation consistent with autosomal recessive inheritance (Fig. 1C). Analysis of the exome outside of the homozygous region revealed no likely causative coding variants.

Patients with p.Leu46Pro substitution in PIG-Y have reduced cell expression of GPI-APs CD55 and CD59 on cultured fibroblasts

Given the known function of PIG-Y, we investigated the effects of the p.Leu46Pro substitution on the surface expression of two GPI-APs, CD55 and CD59. Skin fibroblasts derived from skin biopsies from both affected sisters had a ~20–50% reduction of cell surface expression of CD55 and CD59 compared with three different controls (Fig. 2A) [For CD55-APC: Patient 1, $P = 0.0055$ (mean fluorescence intensity (MFI) = 2809 ± 521), Patient 2, $P = 0.0449$ (MFI = 2393 ± 582) (pooled controls MFI = 3042 ± 485); for CD59-PE: Patient 1, $P = 0.0165$ (MFI = 2422 ± 921), Patient 2, $P = 0.0164$ (MFI = 1927 ± 582) (Pooled control, MFI = 3988 ± 485) using a standard Students' *t*-test]. These data suggest that the PIGY p.Leu46Pro substitution disrupts GPI biosynthesis or interferes with GPI anchoring capacity, associated with reduced expression of CD55 and CD59 on patient cells. Skin fibroblasts were not available from Family B.

Transfection of p.Leu46Pro PIG-Y partially rescues PIG-Y deficient cell line

We permanently transfected Daudi cells (PIG-Y-deficient human Burkitt's lymphoma cell line) with wild-type (WT) or p.Leu46Pro mutant vector constructs driven by the weak promoter followed by assessment of cell surface expression of CD55 and CD59 by FACS analysis. WT-PIG-Y transfection restored the cell surface expression of both CD55 and CD59, but the p.Leu46Pro mutant PIG-Y did not (Fig. 3A). Levels of their expression by the mutant PIGY were similar to the empty vector control. To test if the lack of activity is due to the instability of the mutant PIG-Y protein, stronger (17) expression was needed for detection by western blotting. For this, Daudi cells were transiently transfected with WT or mutant (p.Leu46Pro) pME-oriP HA-PIGY vectors. With this strong promoter-driven vector, the mutant *PIGY* restored the surface expression of CD59 similarly to WT *PIGY*, indicating that the mutant PIG-Y likely has some GPI biosynthetic activity (Fig. 3B). As demonstrated by western blotting, the mutant protein expression was significantly decreased compared with when WT-PIGY was transfected (Fig. 3B). These data suggest that the p.Leu46Pro mutation reduces PIG-Y protein stability leading to lower protein levels and a reduced capacity to synthesize GPI anchors for correct protein targeting to the cell surface.

Patients with p.Leu46Pro substitution in PIG-Y have normal GPI lipid remodelling

Radiolabelling of tritiated mannose into tunicamycin-treated transformed patient fibroblast cells was performed to investigate whether GPI protein anchors in Family A were abnormal in their structure as well as their quantity, as occurs in peroxisomal disorders. GPI precursors in fibroblasts derived from Patients 1 and 2 (Family A) had KOH-resistant alkyl bonds similar to that observed in similarly transformed control fibroblasts (Fig. 3C, bands in KOH lanes). These data suggest that patient cells harbouring the p.Leu46Pro *PIGY* mutation can remodel GPI lipid to the alkyl–acyl form.

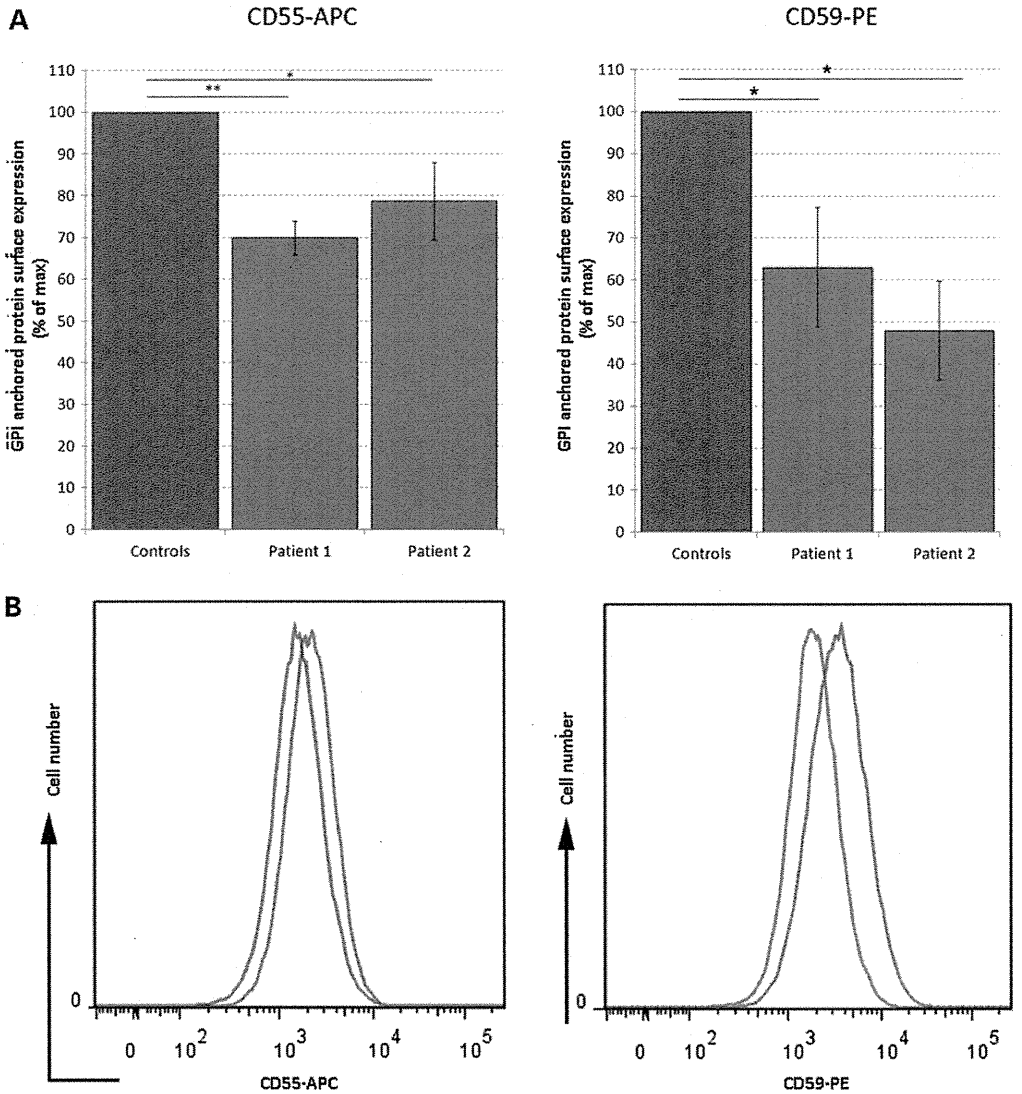

Figure 2. (A) Analysis of patient tissue by flow cytometric analysis. Cultured skin fibroblasts from Patients II-1 and II-2 from Family A were labelled with anti-Human CD55-APC and anti-Human CD59-PE and analysed by flow cytometry. (A) Histograms showing the mean fluorescent intensity (MFI) are depicted for Patient II-1 and show a reduction in MFI for CD55-APC and CD59-PE (red) compared with control (blue). (B) Graphical representation of these data shows a statistically significant reduction in MFI for these GPI markers. Skin fibroblast biopsies were taken from Patient II-1 and Patient II-2 at 5 months and 8 days, respectively. Primary human fibroblast controls were used from three different individuals at ages 5.5 years, 6 months and 3.5 months. All experiments were performed in triplicate.

Effect of c.-540G>A variant on gene expression and GPI anchor biosynthesis

As the c.-540G>A variant disrupts a consensus SP1 transcription factor binding site (GGGGCGGGGC > GGAGCGGGGC) in which there are no other variants reported in dbSNP138, we hypothesized that it might influence *PIGY* gene expression. Sanger sequencing of genomic DNA confirmed that the father (I-1) and the unaffected sibling (II-1) were heterozygous for the A:T haplotype (c.-540G>A:rs3177413) and so could be used to directly compare the relative allelic expression. RT-PCR and Sanger sequencing of two independent blood samples obtained from each of these individuals indicated that expression was consistently higher from the WT allele (data not shown). However, Sanger sequencing does not have a high sensitivity for variant detection when one allele is present at low levels (18). Therefore, to better quantify the relative expression, sequencing was repeated using the Ion Torrent PGM and this showed that only 7–11% of transcripts originate from the mutant allele (Table 1). These results were consistent with qPCR, which showed that for both affected individuals (II-2 and II-3), the *PIGY* expression was at 6–10% compared with an unrelated control (Fig. 4), whereas for the three heterozygote carriers in family B, expression levels were intermediate. Despite this decrease in the *PIGY* transcript levels, we could detect no significant reduction in granulocyte CD16 surface expression for the two individuals homozygous for the c.-540G>A mutation (Supplementary Material, Fig. S3).

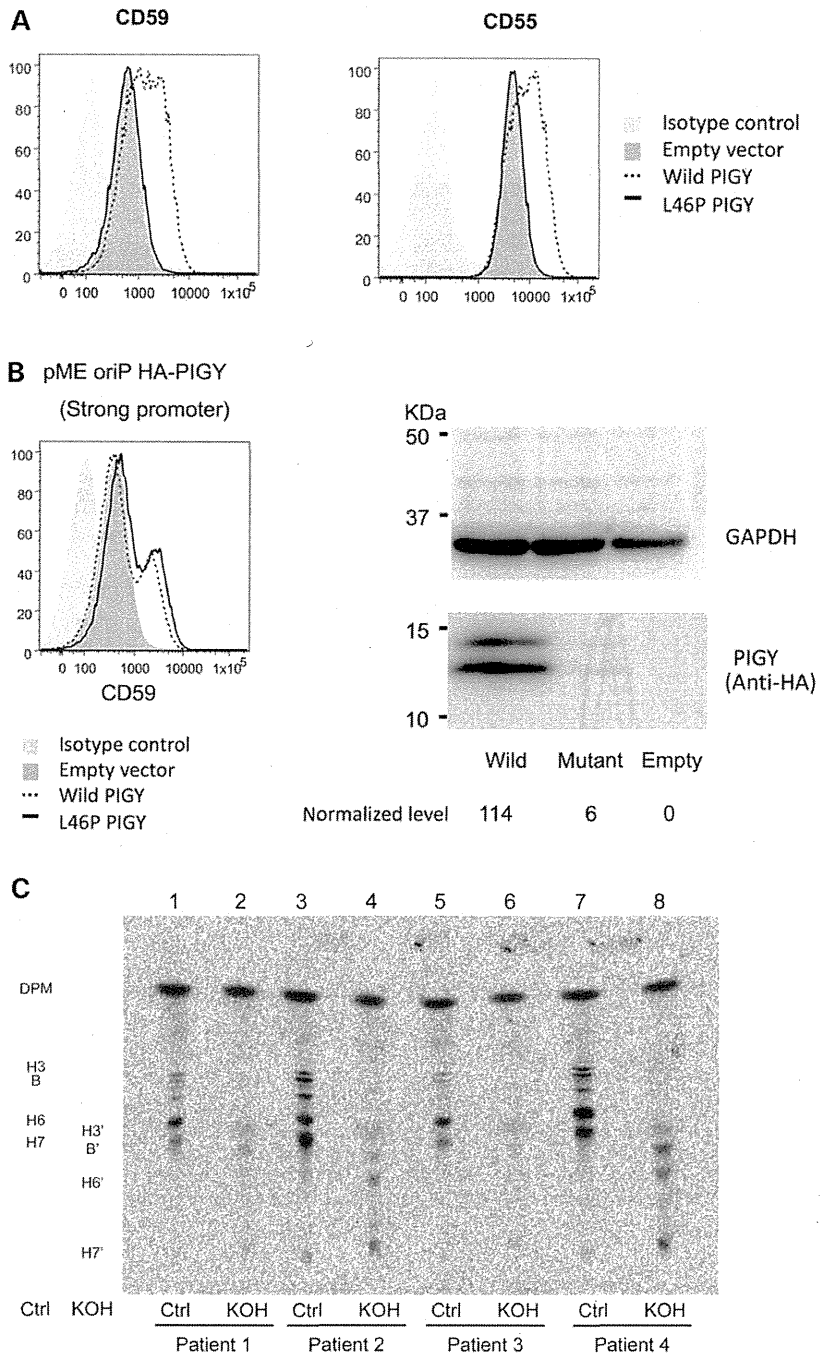

Figure 3. (A) Daudi cells (a PIG-Y deficient human Burkitt's lymphoma cell line) were transiently transfected with normal (WT) or mutant (p.Leu46Pro) PIGY driven by minimum TATA box promoter in pTAL oriP puro *PIGY* (weak promoter). Restoration of the surface expression of CD59 and CD55 was assessed 2 days later by flow cytometry. WT-PIGY restored the surface expression of CD55 and CD59, but p.Leu46Pro mutant PIG-Y did not. (B) After transient transfection of Daudi cells with normal (WT) or mutant (p.Leu46Pro) *PIGY* driven by the strong promoter in pME-oriP HA-PIGY, restoration of surface expression of CD59 was achieved by WT and p. Leu46Pro constructs, indicating that the mutant has some residual activity (left panel). Cell lysates prepared from Daudi cells transfected with either WT-PIGY, mutant p.Leu46Pro *PIGY*, and empty vector were separated by SDS-PAGE and probed for anti-HA and anti-GAPDH antibodies. Normalization of the anti-HA signal compared with GAPDH showed a marked reduction in protein expression in the mutant (p.Leu46Pro) compared with WT. HA-tagged PIG-Y appeared as doublet bands on western blotting for an unknown reason. (C) *In vivo* labelling of ^{3}H-mannose into transformed fibroblast cells derived from Patients II-1 and II-2 (Family A) was performed to enhance incorporation into GPI mannolipids. Fibroblasts derived from Patient 2 (Family A) had KOH-resistant alkyl-bond-containing GPI spots similar to fibroblasts from a healthy control 1 (spots in KOH lanes). Fibroblasts from Patient 1 and another healthy control were not efficiently labelled by mannose. DPM, dolichol-phosphate mannose; H3, B, H6 and H7, mannose-containing GPI precursors; H3′, B7, H6′ and H7′, GPI precursors converted from H3, B, H6 and H7, respectively, by KOH-treatment.

Table 1. Quantitative analysis of *PIGY* allelic expression levels in Family B using Ion Torrent PGM sequencing

Amplicon details			Sample information and genotype			Sequencing rs3177413 on coding strand (CS1)				Sequencing rs3177413 on non-coding strand (CS2)			
Template	Primer sequences (common sequence CS1 and CS2 tags underlined)	Target size	ID	SP1 mutation (c.-540G>A)	rs3177413 (c.-222C>T)	T	C	Total	Percentage T	T	C	Total	Percentage T
cDNA	CS1-PIGY-1Fv2:	232 bp	I-1	A/G	T/C	168	1761	1929	**8.71**	210	2248	2458	**8.54**
	5′-ACACTGACGACATGGTTCTACAGGGGCAAGAAGACTGAGGA-3′;		II-1	A/G	T/C	156	1439	1595	**9.78**	223	1911	2134	**10.45**
	CS2-PIGY-2Rv2:		Control 1	G/G	T/C	981	1190	2171	45.19	1110	1432	2542	43.67
	5′-TACGGTAGCAGAGACTTGGTCTAACTAGCGCTGCTCCACTTC-3′		Control 2	G/G	C/C	2	2078	2080	0.10	2	2099	2101	0.10
			I-2	A/G	T/T	2190	5	2195	99.77	2087	3	2090	99.86
cDNA	CS1-PIGY-1Fv3:	195 bp	I-1	A/G	T/C	544	4361	4905	**11.09**	277	2238	2515	**11.01**
	5′-ACACTGACGACATGGTTCTACAGACCGGGGCAAGAAGACT-3′;		II-1	A/G	T/C	389	4731	5120	**7.60**	160	2072	2232	**7.17**
	CS2-PIGY-2Rv3:		Control 1	G/G	T/C	1899	2006	3905	48.63	1010	973	1983	50.93
	5′-TACGGTAGCAGAGACTTGGTCTTGTCATCCTAGCTGCCTGTG-3′		Control 2	G/G	C/C	9	4787	4796	0.19	1	1387	1388	0.07
			I-2	A/G	T/T	4864	10	4874	99.79	2576	9	2585	99.65
gDNA	CS1-PIGY-intronF:	210 bp	I-1	A/G	T/C	2899	2814	5713	50.74	1988	1625	3613	55.02
	5′-ACACTGACGACATGGTTCTACATGAAAATCAGGCTCTTCAAGC-3′;		II-1	A/G	T/C	2635	2880	5515	47.78	2047	1802	3849	53.18
	CS2-PIGY-2R:		Control 3	G/G	C/C	8	6740	6748	0.12	8	4905	4913	0.16
	5′-TACGGTAGCAGAGACTTGGTCTCTAGCGCTGCTCCACTTCTT-3′		I-2	A/G	T/T	5605	12	5617	99.79	3633	3	3636	99.92

Next generation sequencing of cDNA fragments derived from SP1 mutation carriers confirmed that the mutant *PIGY* allele is expressed at lower levels than the WT allele. As the mutation in the SP1 consensus sequence (located at chr4:89,444,948, hg19) is 4 bp from the transcription start site, this position could not be interrogated directly in cDNA. Instead, the rs3177413 C/T polymorphism was used as a surrogate for the SP1 mutation—familial transmission confirmed that the SP1 mutation is *in cis* with the T allele at rs3177413. Based on raw read counts from two independent cDNA templates, the C/T allelic ratio at rs3177413 (located at chr4: 89 443 162) showed that in heterozygote carriers, only 7–11% of RNA was expressed from the mutant allele (in bold). In contrast, a control subject who was heterozygous for rs3177413 but who did not have the SP1 mutation showed biallelic expression (44–51% from T allele). Sequencing of all samples was performed on a single 314 chip using the Ion Torrent PGM using the Ion Torrent variant caller software after deconvolution of individual sample barcodes. Ion Torrent bidirectional sequencing allows the data derived from the coding and non-coding strands to be analysed independently, and these were shown to be in good agreement with one another. Analysis of genomic DNA from heterozygous samples at rs2177413 were added as internal controls to confirm that there was no amplification or sequencing bias towards one allele, while rs3177413 homozygote samples confirmed that sequencing noise at this position was minimal (<0.2%). Variant positions annotated with reference to NM_001042616.1.

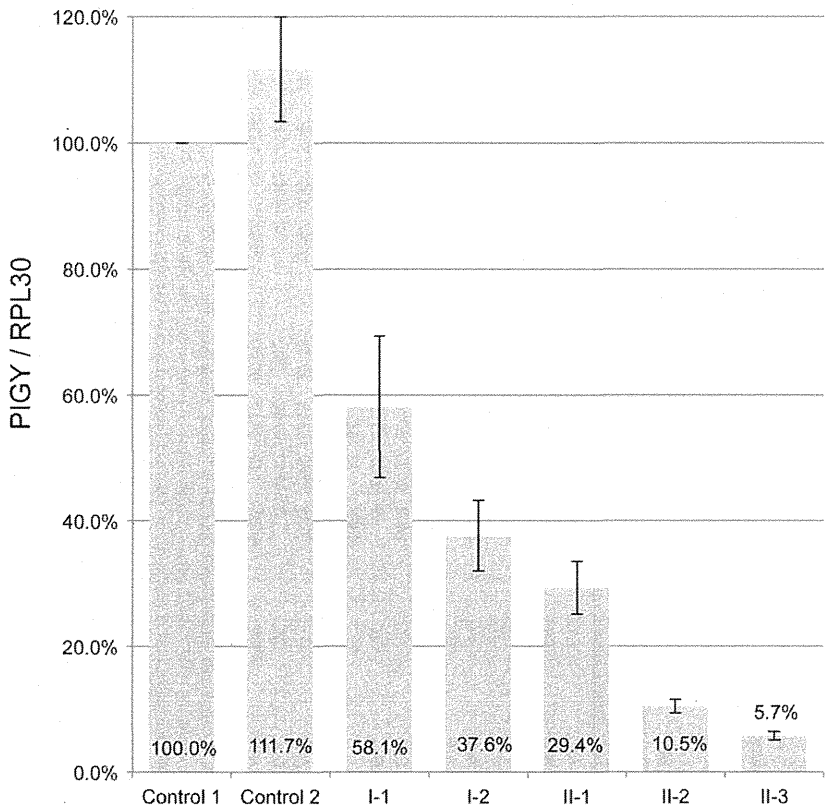

Figure 4. Expression analysis in family B using qPCR. Expression analysis was performed using RPL30 as a control gene, and the results are normalized with respect to the first control individual. qPCRs were performed in triplicate and then the experiment was repeated three times. Error bars represent the standard deviations obtained across the three runs. The RNA used for this experiment was from whole blood samples extracted using the PAXgene blood RNA kit.

Discussion

We describe two families with homozygous recessive mutations in *PIGY*, establishing *PIGY* as a new disease-causing gene in humans. Two affected sisters from Family A, who were homozygous for a missense mutation in *PIGY* (p.Leu46Pro), died from severe multi-system disease while two affected siblings from Family B, homozygous for a mutation in the promoter region of *PIGY* (c.-540G>A), presented with moderate developmental delay and microcephaly. The p.Leu46Pro substitution involves a conserved residue in the second putative transmembrane domain (2). Amino acids in this domain and the carboxy-terminal cytoplasmic region are relatively more conserved among species and may be important for interaction with PIG-A, a catalytic component of GPI-GnT. The substitution of leucine to proline, which is less hydrophobic and is inhibitory to the formation of α-helices, might affect association with PIG-A, thereby causing instability of mutant PIG-Y protein as suggested by our results (Fig. 3B). Fibroblasts derived from both affected sisters from Family A show a 20–50% reduction in protein expression of CD55 and CD59 at the cell surface by flow cytometric assessment, consistent with a defect in GPI-anchor biosynthesis in these patients. Using a cell culture model, we show that expression of mutant p.Leu46Pro PIG-Y in the PIG-Y deficient Daudi cell line only partially restores the cell surface expression of the GPI protein markers CD55 and CD59. Taken together, these results provide strong evidence that the p.Leu46Pro substitution leads to defects in GPI-APs in patient cells.

Family A had multi-system disease consistent with previously described disorders of GPI anchor biosynthesis, whilst Family B had less severe disease limited to microcephaly and global developmental delay. This is likely due to differences in the mutations between the two families and their effects on PIG-Y protein function. We have shown that the promoter mutation in Family B markedly reduces *PIGY* transcript levels in blood, which likely leads to reduced expression of functionally normal PIG-Y protein. We hypothesize that the level of PIG-Y expression in most tissues in Family B is sufficient for many aspects of health, explaining why Family B's phenotype is more limited. The effects of the SP1-binding site mutation on *PIGY* transcript levels may also vary between tissues. Indeed, initial experiments showed no difference in levels of CD16, a GPI-AP, in granulocytes from affected individuals from Family B, suggesting that PIG-Y levels are sufficient for normal GPI biosynthesis in that tissue. The only known cases of GPI deficiency caused by promoter mutations are PIGM deficiency (4). Two individuals with the same homozygous promoter mutation had hepatic vein thrombosis, which has never been reported in GPI deficiency caused by mutations in protein coding regions. It is therefore not surprising that affected individuals from Family B who had homozygous promoter mutation had phenotypes quite different from those of affected individuals from Family A who had mutations in coding region. In contrast, the mutation in Family A will lead to expression of the p.Leu46Pro mutant PIGY protein in all tissues, which likely accounts for the severe, multi-system involvement.

There is growing recognition that autosomal recessive disorders of GPI biosynthesis are an important subclass of the congenital disorders of glycosylation. Over 150 proteins require GPI anchorage for cell-surface expression and all cell types in the body employ this anchoring mechanism (1). Previously published defects of GPI anchor biosynthesis present in infancy with multi-system disease, likely due to the wide range of biological processes affected by the reduced expression of GPI-APs. The findings in our patients help to understand the range of phenotypes that can arise (Table 2). Common dysmorphic features found in a range of GPI anchorage disorders include bi-temporal narrowing, anteverted nares, depressed nasal bridge, long philtrum, high palate and a tented upper lip. The ears are commonly large with fleshy lobes and overfolded helices. Fifth finger clinodactyly and nail hypoplasia are commonly described. Seizures, moderate-to-severe developmental delay, growth failure and cerebral visual impairment are commonly described. Other common features include genitourinary defects, gastrointestinal dysfunction and cardiac defects (Table 1). The sisters from Family A share many features with other inherited GPI anchor defects but are the first to be described with cataracts. The hyperphosphatasia often observed in inherited GPI deficiency occurred albeit mildly in the two affected individuals from Family A. When mature GPI available to precursor alkaline phosphatase was not sufficient, some alkaline phosphatase is transferred to water instead of GPI, resulting in secretion of soluble enzyme. Recently, it has been reported that pyridoxine may be effective in patients with mutations in PIGO (19) and butyrate may be effective in patients with PIGM (20), raising important therapeutic considerations.

The two severely affected patients (Family A) in this study share many clinical features in common with rhizomelic chondrodysplasia punctata type 1 (RCDP1), a peroxisomal disorder which also presents with proximal shortening of the long bones, growth retardation, cataracts, severe intellectual disability, seizures and early death. However, the absence of punctate calcification in our patients is inconsistent with this disorder. Plasmalogens were mildly elevated, phytanic acid was normal and DHAP-AT and DHAP-S activity on cultured skin fibroblasts was normal. Lipid remodelling of GPI anchors occurs in a later part of the GPI biosynthetic pathway and is dependent on the alkyl-phospholipid biosynthetic pathway in the peroxisome. Kanzawa *et al.* showed that patients with mutations in genes involved in peroxisomal biogenesis had defective GPI lipid remodelling and were unable to synthesize 1-alkyl-2-acyl GPIs (21). Unlike patients with RCDP1 and Zellweger syndrome, patients with p.Leu46Pro substitution in PIGY do not have defective GPI lipid remodelling and are able synthesize alkyl–acyl GPI forms. Inherited GPI deficiencies are an important differential for peroxisomal disorders and GPI lipid remodelling might be used as a tool to differentiate between these two clinically similar disorders.

In Family B, even though we could restrict the search space to <1% of the genome based on autozygosity, initial filtering of the 217 641 variants detected by WES did not yield any likely causative variants. It was only after extending our definition of 'deleterious' to include 5′-UTR variants that lie in regions annotated by the ENCODE consortium (22) as transcription factor binding sites, that we uncovered the c.-540G>A variant. UTR regions were not targeted by first-generation exome capture kits and even when capture probes are present in these regions, sequence coverage is often low due to high GC content (Supplementary Material, Fig. S2). Although variants in these regions are becoming less refractory to detection as researchers switch from exome analysis to WGS, they remain difficult to interpret. Our detection of a functional homozygous 5′-UTR variant, despite only having four good quality reads, thus represents an unanticipated finding that highlights the importance of developing better tools to analyse the non-coding portion of the genome.

In conclusion, we describe the first report of two different recessive mutations in the GPI biosynthesis gene *PIGY* that are associated with different phenotypes. The p.Leu46Pro mutation in the coding region of the *PIGY* causes a severe congenital, multisystem disorder resulting in early death, whilst the promoter mutation identified in Family B is associated with a moderate CNS phenotype compatible with life. This study contributes to understanding of the phenotype of disorders associated with deficiencies of the GPI-anchor glycosylation pathway, an important differential diagnosis in infants with multi-system disease, epileptic encephalopathy, dysmorphic facial features, brachytelephalangy and hyperphosphatasia.

Material and Methods

Genetic analysis

This research was approved by the Human Research Ethics Committee of the Children's Hospital at Westmead, Australia (10/CHW/45) and the Wales Research Ethics Committee, UK (12/WA/0001). WES was performed on genomic DNA from two sisters and their parents from Family A in collaboration with the Broad Institute using methods previously reported (23). In Family B, SNP-array-based autozygosity mapping was performed on all close family members using human CytoSNP12v2 (Illumina). WES of the proband (II-2) and data analysis were performed as previously described (24). Segregation of both variants was confirmed by Sanger sequencing.

Cell culture and flow cytometry studies

All tissue culture media and reagents were purchased from Life Technologies unless otherwise stated. Skin fibroblast cells were grown in a Dulbecco's Modified Eagles Media (DMEM)/F12-HAMS supplemented with 10% foetal bovine serum (FBS) and gentamicin (50 μg/ml) and grown in 5% CO_2 incubator. To investigate levels of GPI-APs, cultured skin fibroblasts derived from Patient II-1 in Family A (a full thickness skin biopsy taken at 5 months), Patient II-2 in Family A (8 days) and three controls (ages 3.5 months, 5.5 months and 5.5 years) were treated with versene and incubated with allophycocyanin (APC)-conjugated mouse anti-human CD55 and phycoerythrin (PE)-conjugated mouse anti-human CD59 antibodies (BD Biosciences) in phosphate buffered saline (PBS) without calcium or magnesium and supplemented with 2% FBS for 30 min at 4°C. Cells were then centrifuged at 250*g* for 5 min and washed twice in the above solution. Labelled cells were analysed using a CantoII flow cytometer (BD Biosciences) and analysed using FlowJo™ v 7.6.5 software. Experiments were performed in triplicate from each cell line, and the results were averaged. Fibroblasts were not available from members of Family B and so whole blood samples were used instead. These were treated with ACK lysis buffer and stained with anti-human CD16 (Invitrogen); samples were run on a BD FACSCanto and data analysed by FlowJo. Granulocytes were identified according to FSc and SSc profile.

Functional analysis of mutant PIGY cDNA

Daudi cells (PIG-Y deficient human Burkitt's lymphoma cell line) expressing EBNA1 antigen (2,25) were permanently transfected with WT or c.137T>C mutant PIG-Y constructs containing

Table 2. Comparison with features of described disorders of GPI anchorage

Clinical feature	PIGY Family A (c.137C>T)	PIGY Family B (c.-540G>A)	PIGA (germline mutation)	PIGL	PIGW	PIGM	PIGV	PIGN	PIGO	PIGT
Pregnancy and birth	Polyhydramnios	–						Polyhydramnios		
Dysmorphic features	High forehead, bi-temporal narrowing, upturned nares, depressed nasal bridge, high palate, thick, short neck Fifth finger clinodactyly 2–3 syndactyly	Mildly dysmorphic with long palpebral fissures, bulbous tip to nose, wide mouth, squint	Pierre Robin sequence, depressed nasal bridge, short, anteverted nose, malar flattening, upslanted palpebral fissures, small mouth with downturned corners and a triangular shape, short neck Nail hypoplasia	+	Broad nasal bridge, tented upper lip		Round face, downturned mouth, long palpebral fissures, prominent nasal bridge Nail hypoplasia, hypoplasia of the terminal phalanges Supernumerary nipples	Bi-temporal narrowing, small nose, upturned nares, long philtrum, open mouth, tented upper lip, high palate, micrognathia	Hypertelorism, downward-slanting palpebral fissures, short nose with broad nasal bridge and tip, long philtrum, facial asymmetry, tented mouth Fifth finger clinodactyly Nail hypoplasia Broad distal phalanx of the thumb	High forehead, bi-temporal narrowing, depressed nasal bridge, long philtrum with a deep groove, open mouth
Mild macrosomia and macrocephaly	–	–	+				+	+	–	+
Hypotonia	Truncal hypotonia with brisk reflexes	–	Truncal hypotonia with brisk reflexes	+			+	+		+
Moderate–severe developmental delay	+	+		+	+		+	+	+	+
Growth delay	+	–					+		+	
Seizures	+	–	+	+	Tonic spasms	+	+	+	+	+
Ophthalmologic features	Cataracts cerebral visual impairment	Strabismus		Coloboma			Strabismus	Nystagmus, cerebral visual impairment, wandering eyes	–	Nystagmus, strabismus cerebral visual impairment, hyperopia abnormal eye motility
Ears and hearing		–	Overfolded helix	Conductive hearing loss			Thickened helices	Large ears with fleshy prominent ear lobe, overfolded helix	Large ears with fleshy lobes	Normal hearing
Dental		–	Gingival hypertrophy					Gingival hypertrophy		Premature loss of incisors
Genitourinary tract	Dilated renal collecting systems and increased echogenicity of renal parenchyma	–	Vesicoureteral reflux and a duplicated collecting system		Inguinal hernia		Hydronephrosis	Hydrocele, dilatation of renal collecting system	–	Nephrocalcinosis, ureteral dilatation, unilateral renal cysts and dysplasia

Gastrointestinal	Poor feeding, abdominal distension and vomiting, necrotizing enterocolitis	–				Abdominal distension and vomiting Anterior anus Short-segment Hirschsprung	Feeding and swallowing difficulties. Gastroesophageal reflux. Anal stenosis, imperforate anus, ano-vestibular fistula	Anal stenosis, anal atresia, perineal fistula	
Brain		Small brain	Thin corpus callosum, delayed maturation of white matter, absent septum pellucidum, dilated lateral ventricle, hypoplasia of the cerebellum and vermis				Mild enlargement of ventricular spaces Delayed maturation of white matter and thin corpus callosum. Hypoplasia of the cerebellum and vermis	Enlarged supra-tentorial ventricular system	Variable—frontotemporal atrophy and cerebellar hypoplasia, primitive Sylvian fissures, severe cerebellar atrophy with vermis hypoplasia
Cardiac	–	–	Atrial septal defect, patent ductus arteriosus	Congenital heart disease			Atrial septal defect, peripheral pulmonary stenosis, patent ductus arteriosus	Atrial septal defect, peripheral pulmonary stenosis	Restrictive cardiomyopathy and PDA
Skeletal features	Flexion contractures of the elbows, hip dysplasia. Proximal limb shortening Short fingers and small feet Radiographic—osteopenia, shortening of the small tubular bones of the hands and feet, delayed bone age	–	Craniosynostosis, prominent occiput Hip, knee and elbow contractures. Broad palms with short fingers and poor central tone with brisk reflexes			Brachytelephalangy Mild scoliosis	Tapering fingers, brachydactyly, deep plantar groove between first and second toes, small feet, joint contractures	Brachytelephalangy of digits II–V. Left coronal synostosis	Pectus excavatum, scoliosis, short upper extremities, craniosynostosis Radiographic—bracycephaly, slender and osteopenic long bones with relatively large secondary ossification centres, wide and long femoral necks with enlarged secondary ossification centres, short ulnae and delayed bone age
Haematological		–	Paroxysmal nocturnal haemoglobinuria		Portal and hepatic vein thrombosis		–		

Table continues

Table 2. Continued

Clinical feature	PIGY Family A (c.137C>T)	PIGY Family B (c.-540G>A)	PIGA (germline mutation)	PIGL	PIGW	PIGM	PIGV	PIGN	PIGO	PIGT
Other				Migratory ichthyosiform dermatosis						Atypical lobulation of the lungs Mild elevated of plasma calcium, hypercalciuria and low PTH
ALP	Elevated	Normal			Elevated	–	Elevated	–	Elevated	Low
References			Johnston *et al.* (12)	Ng *et al.* (5)		Almeida *et al.* (4)	Thompson *et al.* 2011	Maydan *et al.* (6)	Krawitz *et al.* (7)	Kvarnung *et al.* (8)

Epstein–Barr virus oriP. For low level expression, *PIGY* cDNA was driven by minimum TATA box promoter in pTAL oriP puro PIGY. Cells (10^7) were suspended in 0.8 ml of Opti-MEM and electroporated with 20 μg each of the plasmids at 350 V and 500 μF using a Gene Pulser (Bio-Rad, Hercules, CA). After selection with 0.5 mg/ml of puromycin for 2 weeks, restoration of the surface expression of GPI-APs was determined by staining cells with mouse anti-human CD59 (5H8), human CD55 antibodies and each isotype IgG followed by a PE-conjugated anti-mouse IgG antibody (mouse IgG1 and IgG2a, and secondary antibody were purchased from BD Biosciences) and analysed by flow cytometer (Canto II) using Flowjo software (Tommy Digital Inc., Tokyo, Japan). For high level expression, PIG-Y deficient Daudi cells were transiently transfected with WT or mutant (c.137T>C) strong promoter-driven pME-oriP HA-PIGY. Two days later, restoration of the surface expression of CD59 was assessed by flow cytometry. Lysates were applied to SDS-PAGE, and western blotting was performed using anti-HA antibody (HA-7, Sigma, St. Louis, MO). The levels of protein expression were normalized with the intensities of glyceraldehyde-phosphate dehydrogenase (GAPDH), the loading control and luciferase activities used for evaluating transfection efficiencies.

GPI mannolipid analysis

Patient and control fibroblasts were transformed using telomerase gene and SV40 large T gene and metabolically radiolabeled with tritiated mannose in the presence of tunicamycin to enhance incorporation into GPI mannolipids by preventing incorporation into more abundant N-glycan precursors. Radiolabeled GPI mannolipids were treated with 0.1 N KOH to cleave ester linkages and then analysed by thin layer chromatography on silica gel followed by phosphoimaging to detect tritiated GPI (26).

Gene expression analysis

RNA was extracted from 2.5 ml of blood using the PAXgene kit (Qiagen) and Reverse Transcriptase (RT) reactions were performed using the QuantiTect RT kit (Qiagen). Relative allelic expression of *PIGY* was measured by analysing cDNA using both Sanger sequencing and a 314 chip run on the Ion Torrent PGM platform. As the c.-540G>A variant is only 4 bp from the transcription start site, expression levels had to be measured indirectly using the T allele at rs3177413 (c.-222C>T) which familial transmission showed was *in cis* with c.-540G>A allele. RT-PCR primer sequences are shown in Table 1. The first round of amplification (25–30 cycles) and second round of amplification (15 cycles, with barcoding primers) were both performed with the FastStart Taq DNA polymerase kit (Roche). Samples were pooled, cleaned using Ampure beads, quantified using the BioAnalyser (Agilent) and diluted to 10 pM. Emulsion PCR and sequencing were carried out according to manufacturer instructions.

Quantitative PCR was performed using IQ SYBR Green Supermix (BIO-RAD) and the iQ5 Real-Time PCR Detection System (BIO-RAD) and the following primers: PIGY-V5-F 5′-AGG GATGTTCATCTCCAACCA-3′, PIGY-V5-R 5′-TGCGCATATCAGGCT TAGGA-3′, RPL30-F 5′-CAGACAAGGCAAAGCGAAAT-3′ and RPL30-R 5′-TGGACACCAGTTTTAGCCAAC-3′. PCRs were performed in triplicate, and the experiment was carried out three times.

Authors contributions

Sydney, Australia Group

The Sydney Group lead by Nigel Clarke (senior author) identified the gene and lead the collaborative studies to ascribe

pathogenicity. Both Nigel Clarke and Kathryn North were responsible for study concept and design, analysis and interpretation of data, study supervision obtaining funding and drafting/revising manuscript for content. Biljana Ilkovski's (co-first author) contribution has been to perform the flow cytometric experiments on the patient cells (Fig. 2), assemble the figures and take a lead role in the preparation of the manuscript. Gina O'Grady (author position #2) identified the gene via WES, confirmed the mutation and family inheritance, reviewed and assembled detailed clinical and pathological information, compiled a detailed clinical table of all known PIG phenotypes, helped write and edit the manuscript. Leigh Waddell was involved in mutation identification and confirmed the mutation by Sanger Sequencing and edited the manuscript. Fabienne Brilot helped direct flow cytometeric experiments and edited the manuscript. David Sillence, Anne Turner and John Christodoulou were the clinicians who described the clinical phenotypes of the patients, contributed to diagnostic investigations and edited the manuscript.

UK Group

The Oxford Group lead by Usha Kini and Jenny Taylor identified the gene in the UK family. Alistair Pagnamenta (co-first author) performed SNP array experiments, homozygosity mapping, analysed exome data, did RNA extractions, designed and performed RNA sequencing, was involved in the flow cytometry experiments and helped write and edit the manuscript. Malcolm Howard performed the qPCR and Sanger validation of the UK Family mutation, analysed exome data and helped with the flow cytometry. Samantha Knight supervised and reviewed the SNP array data. Consuelo Anzilotti helped perform the flow cytometry experiments. Anne Goriely helped design, perform and interpret data from the PGM RNA sequencing experiment. Niko Popitsch analysed the exome coverage in the two families and compared with in house WGS data. David Keays was involved with setting up of the Oxford Brain Abnormalities group.

Boston, USA Group

The Boston Group lead by Daniel MacArthur identified the gene in the Australian family via WES. Monkol Lek and Brett Thomas performed the Bioinformatics of WES to ascribe pathogenicity. All authors revised and edited the manuscript.

Japanese Group

The Japanese Group lead by Taroh Kinoshita lead the collaborative studies to examine the functional consequences of the PIGY mutation in the Australian family using cell culture models lipid remodelling studies, helped write and edit the manuscript. Yoshiko Murakami and Noriyuki Kanzawa were responsible for designing the flow cytometric experiments examining expression of PIG-Y constructs into PIG-Y deficient cells as well as the lipid remodelling studies and helped write and edit the manuscript.

Supplementary Material

Supplementary Material is available at *HMG* online.

Acknowledgements

We thank the families for their contributions and Indira Taylor for technical assistance. The views expressed in this publication are those of the authors and not necessarily those of the Department of Health.

Conflicts of Interest statement. None declared.

Funding

This work was supported by the National Health & Medical Research Council of Australia (APP571287—KN, NC, APP1035828—NC and APP1022707—KN, NC) and National Institute for Health Research (NIHR) Biomedical Research Centre Oxford with funding from the Department of Health's NIHR Biomedical Research Centres funding scheme. We thank the High-Throughput Genomics Group at the Wellcome Trust Centre for Human Genetics (funded by Wellcome Trust grant reference 090532/Z/09/Z and Medical Research Council Hub grant G0900747 91070) for generating the sequencing data. Funding to pay the Open Access publication charges for this article was provided by the Wellcome Trust.

References

1. Kinoshita, T., Fujita, M. and Maeda, Y. (2008) Biosynthesis, remodelling and functions of mammalian GPI-anchored proteins: recent progress. *J. Biochem.*, **144**, 287–294.
2. Murakami, Y., Siripanyaphinyo, U., Hong, Y., Tashima, Y., Maeda, Y. and Kinoshita, T. (2005) The initial enzyme for glycosylphosphatidylinositol biosynthesis requires PIG-Y, a seventh component. *Mol. Biol. Cell.*, **16**, 5236–5246.
3. Takeda, J., Miyata, T., Kawagoe, K., Iida, Y., Endo, Y., Fujita, T., Takahashi, M., Kitani, T. and Kinoshita, T. (1993) Deficiency of the GPI anchor caused by a somatic mutation of the PIG-A gene in paroxysmal nocturnal hemoglobinuria. *Cell*, **73**, 703–711.
4. Almeida, A.M., Murakami, Y., Layton, D.M., Hillmen, P., Sellick, G.S., Maeda, Y., Richards, S., Patterson, S., Kotsianidis, I., Mollica, L. *et al.* (2006) Hypomorphic promoter mutation in PIGM causes inherited glycosylphosphatidylinositol deficiency. *Nat. Med.*, **12**, 846–851.
5. Ng, B.G., Hackmann, K., Jones, M.A., Eroshkin, A.M., He, P., Wiliams, R., Bhide, S., Cantagrel, V., Gleeson, J.G., Paller, A.S. *et al.* (2012) Mutations in the glycosylphosphatidylinositol gene PIGL cause CHIME syndrome. *Am. J. Hum. Genet.*, **90**, 685–688.
6. Maydan, G., Noyman, I., Har-Zahav, A., Neriah, Z.B., Pasmanik-Chor, M., Yeheskel, A., Albin-Kaplanski, A., Maya, I., Magal, N., Birk, E. *et al.* (2011) Multiple congenital anomalies-hypotonia-seizures syndrome is caused by a mutation in PIGN. *J. Med. Genet.*, **48**, 383–389.
7. Krawitz, P.M., Murakami, Y., Hecht, J., Krüger, U., Holder, S.E., Mortier, G.R., Delle Chiaie, B., De Baere, E., Thompson, M.D., Roscioli, T. *et al.* (2012) Mutations in PIGO, a member of the GPI-anchor-synthesis pathway, cause hyperphosphatasia with mental retardation. *Am. J. Hum. Genet.*, **91**, 146–151.
8. Kvarnung, M., Nilsson, D., Lindstrand, A., Korenke, G.C., Chiang, S.C., Blennow, E., Bergmann, M., Stödberg, T., Mäkitie, O., Anderlid, B.M. *et al.* (2013) A novel intellectual disability syndrome caused by GPI anchor deficiency due to homozygous mutations in PIGT. *J. Med. Genet.*, **50**, 521–528.
9. Horn, D., Wieczorek, D., Metcalfe, K., Barić, I., Paležac, L., Cuk, M., Petković Ramadža, D., Krüger, U., Demuth, S., Heinritz, W. *et al.* (2014) Delineation of PIGV mutation spectrum and associated phenotypes in hyperphosphatasia with mental retardation syndrome. *Eur. J. Hum. Genet.*, **22**, 762–767.
10. Chiyonobu, T., Inoue, N., Morimoto, M., Kinoshita, T. and Murakami, Y. (2014) Glycosylphosphatidylinositol (GPI)

anchor deficiency caused by mutations in PIGW is associated with West syndrome and hyperphosphatasia with mental retardation syndrome. *J. Med. Genet.*, **51**, 203–207.
11. Martin, H.C., Kim, G.E., Pagnamenta, A.T., Murakami, Y., Carvill, G.L., Meyer, E., Copley, R.R., Rimmer, A., Barcia, G., Fleming, M.R. *et al.* (2014) Clinical whole-genome sequencing in severe early-onset epilepsy reveals new genes and improves molecular diagnosis. *Hum. Mol. Genet.*, **23**, 3200–3211.
12. Johnston, J.J., Gropman, A.L., Sapp, J.C., Teer, J.K., Martin, J.M., Liu, C.F., Yuan, X., Ye, Z., Cheng, L., Brodsky, R.A. and Biesecker, L.G. (2012) The phenotype of a germline mutation in PIGA: the gene somatically mutated in paroxysmal nocturnal hemoglobinuria. *Am. J. Hum. Genet.*, **90**, 295–300.
13. Sutherland, D.R., Kuek, N., Davidson, J., Barth, D., Chang, H., Yeo, E., Bamford, S., Chin-Yee, I. and Keeney, M. (2007) Diagnosing PNH with FLAER and multiparameter flow cytometry. *Cytometry B. Clin. Cytom.*, **72**, 167–177.
14. Adzhubei, I.A., Schmidt, S., Peshkin, L., Ramensky, V.E., Gerasimova, A., Bork, P., Kondrashov, A.S. and Sunyaev, S.R. (2010) A method and server for predicting damaging missense mutations. *Nat. Methods*, **7**, 248–249.
15. 1000 Genomes Project ConsortiumAbecasis, G.R., Auton, A., Brooks, L.D., DePristo, M.A., Durbin, R.M., Handsaker, R.E., Kang, H.M., Marth, G.T. and McVean, G.A. (2012) An integrated map of genetic variation from 1,092 human genomes. *Nature*, **491**, 56–65.
16. Tennessen, J.A., Bigham, A.W., O'Connor, T.D., Fu, W., Kenny, E.E., Gravel, S., McGee, S., Do, R., Liu, X., Jun, G. *et al.* (2012) Evolution and functional impact of rare coding variation from deep sequencing of human exomes. *Science*, **337**, 64–69.
17. Takebe, Y., Seiki, M., Fujisawa, J., Hoy, P., Yokota, K., Arai, K., Yoshida, M. and Arai, N. (1988) SR alpha promoter: an efficient and versatile mammalian cDNA expression system composed of the simian virus 40 early promoter and the R-U5 segment of human T-cell leukemia virus type 1 long terminal repeat. *Mol. Cell Biol.*, **8**, 466–472.
18. Rohlin, A., Wernersson, J., Engwall, Y., Wiklund, L., Bjork, J. and Nordling, M. (2009) Parallel sequencing used in detection of mosaic mutations: comparison with four diagnostic DNA screening techniques. *Hum. Mutat.*, **30**, 1012–1020.
19. Kuki, I., Takahashi, Y., Okazaki, S., Kawawaki, H., Ehara, E., Inoue, N., Kinoshita, T. and Murakami, Y. (2013) Vitamin B6-responsive epilepsy due to inherited GPI deficiency. *Neurology*, **81**, 1467–1469.
20. Almeida, A.M., Murakami, Y., Baker, A., Maeda, Y., Roberts, I. A., Kinoshita, T., Layton, D.M. and Karadimitris, A. (2007) Targeted therapy for inherited GPI deficiency. *N. Engl. J. Med.*, **356**, 1641–1647.
21. Kanzawa, N., Shimozawa, N., Wanders, R.J., Ikeda, K., Murakami, Y., Waterham, H.R., Mukai, S., Fujita, M., Maeda, Y., Taguchi, R. *et al.* (2012) Defective lipid remodeling of GPI anchors in peroxisomal disorders, Zellweger syndrome, and rhizomelic chondrodysplasia punctata. *J. Lipid. Res.*, **53**, 653–663.
22. ENCODE Project Consortium, Collaborators (594). (2012) An integrated encyclopedia of DNA elements in the human genome. *Nature*, **489**, 57–74.
23. Menezes, M.P., Waddell, L., Lenk, G.M., Kaur, S., MacArthur, D. G., Meisler, M.H. and Clarke, N.F. (2014) Whole exome sequencing identifies three recessive FIG4 mutations in an apparently dominant pedigree with Charcot-Marie-Tooth disease. *Neuromuscul. Disord.*, **24**, 666–670.
24. Howard, M.F., Murakami, Y., Pagnamenta, A.T., Daumer-Haas, C., Fischer, B., Hecht, J., Keays, D.A., Knight, S.J., Kölsch, U., Krüger, U. *et al.* (2014) Mutations in PGAP3 impair GPI-anchor maturation, causing a subtype of hyperphosphatasia with mental retardation. *Am. J. Hum. Genet.*, **94**, 278–287.
25. Canitano, A., Venturi, G., Borghi, M., Ammendolia, M.G. and Fais, S. (2013) Exosomes released in vitro from Epstein-Barr virus (EBV)-infected cells contain EBV-encoded latent phase mRNAs. *Cancer Lett.*, **337**, 193–199.
26. Kanzawa, N., Maeda, Y., Ogiso, H., Murakami, Y., Taguchi, R. and Kinoshita, T. (2009) Peroxisome dependency of alkyl-containing GPI-anchor biosynthesis in the endoplasmic reticulum. *Proc. Natl. Acad. Sci. USA*, **106**, 17711–17716.